Exploring the Properties of Zr2CO2/GaS Van der Waals Heterostructures for Optoelectronic Applications

Abdul Abdul (✉ mabdul@mail.ustc.edu.cn)

University of Science and Technology of China, Hefei, People's Republic of China

Altaf Ur Rahman Khan

University of Electronic Science and Technology of China

Jing Bo

University of Electronic Science and Technology of China

Jehan Akbar Khan

University of Glasgow

Qammer H. Abbasi

University of Glasgow,

Bao JingFu

University of Electronic Science and Technology of China, Sichuan Chengdu, China

---

Article

Additional Declarations: (Not answered)

Exploring the properties of Zr_2CO_2/GaS van der Waals heterostructures for Optoelectronic Applications

Altaf Ur Rahman,[1] JingBo,[1] Jehan Akbar,[2] Qammer H. Abbasi,[2] M. Abdul,[3, *] and Bao JingFu[4, †]

[1]*Institute of Fundamental and Frontier Sciences,*
University of Electronic Science and Technology of China

[2]*James Watt School of Engineering, University of Glasgow, Uk*

[3]*Division of Quantum Physics and Quantum Information, Department of Modern Physics,*
University of Science and Technology of China, Hefei, People's Republic of China

[4]*School of Integrated Circuit Science and Engineering,*
University of Electronic Science and Technology of China, Sichuan Chengdu, China

(Dated: November 8, 2023)

Abstract

We investigate the structural, electronic and optical properties of eight possible Zr_2CO_2/GaS van der Waals heterostructures using first-principles calculations. These structures display favorable stability, indicated by matching crystal structures and a negative formation energy (-6.57 eV). In all configurations, they act as indirect bandgap semiconductors with a type-II band alignment, allowing efficient electron-hole separation. Optical studies reveal their suitability for optoelectronic applications. Zr_2CO_2/GaS under 3% biaxial compressive strain meets the criteria for photocatalytic water splitting, suggesting their potential for electronic and optoelectronic devices in the visible spectrum. Our findings present prospects for advanced photocatalytic materials and optical devices.

Keywords: Density Functional Theory, Hybrid Functional Calculations, Two-dimensional Materials, Van der Waals Heterostructure, Electronic and Optical Properties.

* mabdul@mail.ustc.edu.cn

† baojingfu@uestc.edu.cn

I. INTRODUCTION

The successful exfoliation of graphene, which is known as the first two-dimensional (2D) material, got attention in the ever changing nanotechnology world to offer the innovative solutions for the next generations breed of nano-electronic devices. Particularly the new family of 2D materials referenced as MXenes, composed of transition metal element (M), carbides, nitrides, and carbonitrides. Mxenes have drawn growing interest due to their exceptional electronic, spintronic, thermal and optical properties, making them promise for efficient photocatalytic water splitting, nanoelectronic and optical instruments applications [1, 2]. Transition metal carbides is a novel class of 2D layered materials with significant inter-layer bonding as opposed to van der Waals (vdW) bonding; for instance, in three-dimensional (3D) stacked sheets of carbon atoms known is graphite, the carbon atomic layers are connected by weak vdW bonding [3, 4].

In layered materials, the long range vdW interactions as seen in the 3D bulk layered materials make mechanical exfoliation possible. As a result, majority of the 2D monolayers are exfoliated from 3D bulk layered materials. Recently, Y. Gogotsi *et al*, reported experimental results making a MXene with five atomic layers of transition metals and its MAX phase precursor, which contains no additional MAX phase impurities [5]. Naguib *et al*, showed that chemical etching procedures could also exfoliate 3D nanolaminate MAX phases with covalent interlayer bonding into a 2D monolayer [6]. This finding makes the synthesise possible for many other 2D materials.

The name "MXene" is derived from its structure: "M" represents the transition metal, "X" represents carbon and/or nitrogen, and "ene" indicates its two-dimensional nature. The generic formula for 2D MXenes materials is $M_{n+1}X_nT$, where M stands for early transition-metals (Ti, Zr, etc.), whereas X stands for carbon (C) or nitrogen (N) atom, "T" represents surface terminations group elements, usually functional groups like hydroxyl or fluorine, and n denotes the number of layers which can take integer values 1, 2, or 3. The MXene monolayer has a thickness of about one nanometer, which increases with the increase value of n and the type of functionalization component, may be atom, may be a molecule such as $-O$, $-OH$, $-F$, $-Cl$, etc [6–8]. In the MAC/N phase, the $M-C/N$ bond interaction is stronger than the M-A interaction. In order to produce 2D MXene, hydrogen fluoride (HF) acid is added which can readily disintegrate the metallic layers of A atoms. Recently, a variety of MAX compounds based on Boron (B) are predicted [9]. The crystal structural, elastic, electrical, thermoelectric, and optical properties of MXenes both with and without the surface terminations were investigated [6, 10–12]. Due to their diverse structural and compositional properties, MXenes are promising candidates for a range of

applications, including energy storage devices [13, 14] such as catalysts [15], sensing devices[16], transparent conductors [17], hydrogen storage [13], and thermoelectric materials [18, 19],

The vdW heterostructure is synthesized by stacking two layers of different layered materials with weak interlayer interactions, which have interesting electronic properties to fulfill the requirements of nanoelectronic devices [20]. Due to weak interaction between the layers, each material's intrinsic electrical characteristics is maintained in the heterostructure, and the novelty of physics can be seen playing its role onle at the interface.

Based on the exploitation of the novel interfacial phenomenon, it has been demonstrated theoretically and experimentally that type-II band alignment of vdWs heterostructures can be used for solar energy conversion, such as TiO_2/V_2O_5 vdWs heterostructures [21, 22]. The vdW heterostructure with type-II band alignment can be used to separate electron and holes in different monolayer. Such type of heterostructure have demanding applications in solar cell and photocatalic devices. However, 2D vdWs heterostructures, which are capable of turning solar energy into electricity, can also be used as a renewable energy source [23–25]. Further in this quest, 2D MXenes materials demonstrate increased efficiency when used for energy conversion. Academics' interest in sunlight energy conversion into electricity based on electronic gadgets has long been piqued. The electronic and optical properties of potential materials are therefore being improved and demonstrated both theoretically and practically. For example, $Zr_2CO_2/MoSe_2$ heterostructure form a type-II band alignment. The photocatalytic efficiency of $Zr_2\ CO_2/MoSe_2$ heterostructure is generally enhanced under strain [12]. As a result, combining MXenes with other 2D materials is a successful method for creating MXene/2D hybrids with fascinating performance. The reported electronic properties of $Zr_2CO_2/MoSe_2$ vdw Waals heterostructures under biaxial strain $−2$ % to 9 % indicates that the bandgap lye in the range of 0 eV to 1.25 eV [12]. For optical application we need bandgap in the visible range of value equale to or above 1.40 eV. So the reported $Zr_2CO_2/MoSe_2$ vdw Waals hetrostructure has a bandgap proplem for optical numerious applications. We focus on Zr_2CO_2 interfaced with GaS monolayer because the isolated GaS monolayer has a large bandgap as compared to isolated $MoSe_2$ monolayer. So we expect the desired results for optical application by considering the Zr_2CO_2/GaS vdw Waals heterostructures.

As we know, the optical efficiency of a material for photocatalytic applications is frequently determined through the absorption of photon energy. Strong optical conductivity and absorption coefficient is needed for a material to be used in practical applications. The optical efficiency of 2D materials can be raised by: (i) tuning the electronic band gap below 3 eV through stack-

ing them together with different 2D materials, and (ii) improving optical absorption coefficient. Additionally, the development of a vdWs heterostructures yields improved electrical and optical properties in comparison to the individual monolayers. Using density functional theory (DFT), new photocatalytic materials are studied. Realizing a 2D materials with outstanding electronic and optical properties is challenging, despite theoretical and practical attempts to predict a prospective candidate for efficient optoelectronic devices. This study focuses on the electronic and optical properties of isolated Zr2CO2, GaS monolayers, and Zr2CO2/GaS vdW heterostructures with a hope to propose and make it suitable for optoelectronic devices. We will investigate how the optical properties are changed when the material interacts with incoming photon of different energies. In addition, we will also focus on how strain can come into play affecting the alignment of the bands of Zr2CO2/GaS vdW heterostructures.

II. COMPUTATIONAL METHODS AND MODELING

All the calculations were carried out in the framework of Density functional theory (DFT) [26] as implemented in the Quantum Espresso (QE) package [27]. The plane-wave and ultra-soft pseudo-potentials were used to perform the calculations. We used the generalized gradient approximation (GGA) calculating the exchange correlation interactions proposed by Perdew, Burke, and Ernzer-hof (PBE) [28]. The electron wave functions were expressed in term of a plane wave basis set with kinetic energy and charge density cutoffs of value 60 Ry and 300 Ry, respectively.

The Monkhorst-Pack method [29] was used for creating k-meshes in the first Brillouin-zone (BZ). A $12 \times 12 \times 1$ k-mesh was employed for geometric optimization, whereas a dense $20 \times 20 \times 1$ k-mesh was employed to calculate the total density of states (TDOS) and the optical characteristics of both isolated monolayers and vdW heterostructures. The van vdW interaction between the slabs was treated using the Grimme DFT-D2 correction. It is necessary to employ a vacuum thickness greater than 15 Å to prevent the interactions between the adjacent slabs. We thoroughly examined the convergence of results for each and every computational parameter. For crystal structure optimization, all the atomic position of atoms were permit to relax until the Hellmann-Feynman forces were get smaller than 0.003 Ry/Bohr. We estimated the formation energy to ensure structural integrity, which is defined as

$$E_f = \{E_{\text{tot}[Zr_2CO_2]} - 2E_{\text{tot}[Zr]} - 2E_{\text{tot}[O]} - E_{\text{tot}[C]}\}) \tag{1}$$

where $E_{\text{tot}[Zr_2CO_2]}$ represent the ground state energy of Zr_2CO_2 monolayer and $E_{\text{tot}[Zr]}$, $E_{\text{tot}[C]}$,

and $E_{tot[O]}$ represents the ground state energy per zirconium atom, carbon atom and oxygen atoms in its lowest chemical-potential phase, respectively. The lowest chemical-potential of the Zr/C atom is calculated using its natural occurring phase (HCP: Hexagonal Closed Packed), which consists of two constituent atoms in its primitive unit cell. The total energy of the oxygen molecule (O_2), which consists of two atoms of oxygen is utilized to determine the total energy of atomic oxygen. The accuracy of electronic characteristics is essential for determining the catalytic mechanism of GaS and Zr_2CO_2 monolayers as well as the Zr_2CO_2/GaS van der Waal heterostructures. It is well known that the GGA+PBE energy functional typically underestimates the semiconductor band gap [22]. Therefore, in order to precisely calculate the electrical and optical characteristics of 2D GaS, Zr_2CO_2, and Zr_2CO_2/GaS van der Waal heterostructure, we used Heyd–Scuseria–Ernzerhof (HSE) functional [30]. We employed the hybrid functional to solve the band gap problem by combining the Hartree-Fock and DFT exchange terms [31]. The mixing parameter governing how much Hartree-Fock exchange is incorporated in the hybrid functional is called the "fraction of exchange" (α). To increase the precision of electronic structure calculations, the semi-local and non-local screened Hartree-Fock exchange combined in the HSE hybrid functional. If = 0.20, then 80 % of semi-local and 20 % of Hartree-Fock exchanges are combined. For HSE calculations, the fraction of exchange (α) of amount 0.20 and exchange screening parameter (β) set to 0.12 are used which can reproduce the experimental bandgap of GaS, Zr_2CO_2 monolayers and Zr_2CO_2/GaS van der Waal heterostructures.

Optical properties of materials are important for potential use in optical devices and electronic detectors. When electromagnetic radiation passes through a material then various phenomena take place due to the interaction light-matter such as reflection, transmission, and absorption. Optical characteristics of a materials are investigated in terms of these parameters [32, 33]. Among which, one of the important and basic parameters is the complex part of the dielectric function $\epsilon(\omega)$. The complex part $\epsilon_2(\omega)$ is directly related to the material linear response to solar light irradiation. The dielectric function $\epsilon(\omega)$ is expressed in terms of real $\epsilon_1(\omega)$ and complex parts $\epsilon_2(\omega)$ mathematically as;

$$\epsilon(\omega) = \epsilon_1(\omega) + \iota\epsilon_2(\omega) \tag{2}$$

The imaginary part $\epsilon_2(\omega)$ contain the information about how much total energy of the incident photon is absorbed by system. The complex part can be obtained using the basis of RPA (RPA:

Random Phase Approximation) [34, 35];

$$\epsilon_2(\omega) = \frac{4\pi^2 e^2}{m^2 \omega^2} \sum_{i,j} \int_k \langle i|M|j\rangle^2 f_i (1 - f_i) \times \delta(E_{j,k} - E_{i,k} - \omega) d^3 k \tag{3}$$

Here, the integrand represents the dipole matrix, i and j represent ground and excited states, the corresponding ground state energy indicated by E_i, excited state energy indicated by E_f and f_i denotes the Fermi-distribution function of the ground level. To connect mathematically the real and imaginary part of the dielectric functions the set of Kramers-Kronig relations are used [36]. This can be mathematically expressed as;

$$\epsilon_1(\omega) = 1 + \frac{2}{\pi} P \int_0^\infty \frac{\omega' \epsilon_2(\omega')}{(\omega'^2 - \omega^2)} d\omega \tag{4}$$

The improper value of the above integral is captured by the Cauchy principle value denoted by P. The other optical parameter can be expressed in term of $\epsilon_1(\omega)$ and $\epsilon_2(\omega)$. To characterize how incident photon interacts with a material, we can define index of refraction which is itself a complex quantity consisting of both real and imaginary parts, the real part know is refractive index and imaginary part termed as extinction coefficient [37]. Mathematically it can be expressed as;

$$\bar{n}(\omega) = n(\omega) + \iota k(\omega) \tag{5}$$

The real part of the index of refraction tells us how much the speed of an incident photon slows down as it passes through a material compared to the speed of light. The imaginary part describing attenuation (absorption) of incident photon as it passes through material medium [38]. The refractive index and extinction coefficients can be written in term of $\epsilon_1(\omega)$ and $\epsilon_2(\omega)$, as given below

$$n(\omega) = (1/\sqrt{2}) \left[\sqrt{\epsilon_1^2(\omega) + \epsilon_2^2(\omega)} + \epsilon_1(\omega) \right]^{1/2} \tag{6}$$

and

$$k(\omega) = (1/\sqrt{2}) \left[\sqrt{\epsilon_1^2(\omega) + \epsilon_2^2(\omega)} - \epsilon_1(\omega) \right]^{1/2} \tag{7}$$

Similarly, to measure how much incident photon energy is reflected back from a material surface rather than being absorbed, we can define reflection coefficient $R(\omega)$ [39], The $R(\omega)$ can be derived from in real and imaginary part of the index of refraction. $R(\omega)$ as given below:

$$R(\omega) = \frac{(1 - n)^2 + k^2}{(1 + n)^2 + k^2} \tag{8}$$

$$L(\omega) = \frac{\epsilon_2(\omega)}{\epsilon_1^2(\omega) + \epsilon_2^2(\omega)} \tag{9}$$

6

Here $L(\omega)$ is electron energy loss function [40] which is derived from the $\epsilon_1(\omega)$ and $\epsilon_2(\omega)$. An electron energy loss function is an essential idea in materials science and condensed matter physics is the electron energy loss function (EELF). It accounts for the energy that is lost by an incident electron as it travels through a substance as a result of interactions with the electrons in the substance. This phenomenon is frequently seen via experimental methods like electron energy loss spectroscopy (EELS) [40], and it has applications in a number of disciplines, such as solid-state physics, surface science, and nanotechnology.

III. RESULTS AND DISCUSSIONS

A. Pristine Zr_2CO_2 and GaS monolayers

We optimized the crystal structures of GaS and Zr_2CO_2 monolayers, which belong to hexagonal structures with the P6_3/mmc space group. We first used the Perdew-Burke-Ernzerhof (PBE) exchange-correction energy functional with the Grimme (DFT-D2) method [41] to calculate the lattice parameters of GaS and Zr_2CO_2 monolayers. Following our previous work, which is based on the lattice site of the functional atom oxygen (O), four possible configurations of Zr_2CO_2 monolayers, termed MD1, MD2, MD3, and MD4, were considered [18].

Rahman *et al,* considered different possible models for Zr_2CO_2 monolayer and reported optimized planer lattice geometry with a$_o$ is 3.36 Å , 3.61 Å , 3.31 Å , 3.24 Å and 3.25 Å , for MD-0, MD-1, MD-2, MD-3, and MD-4 configurations, respectively [18]. Here, the lattice constant optimization plot [see Figure SI2] indicates that Zr_2CO_2 monolayer [MD4 configuration as shown in the Figure SI1(a, b)] has optimized lattice constant of 3.25 Å to be consistent with previously reported values [12]. Previously MD2 configuration is found to be the most stable, but here the material is stable in all possible configurations. The optimized Zr−−C bond length (denoted as b_{Zr-C}) is changes slightly with the functionalization of oxygen atoms at varying position from top and bottom surfaces.

By changing the termination position of oxygen atom, Zr−− bond length (denoted as b_{Zr-O}) is enhanced (see table I. These observations about a$_o$, bond length are in line with the earlier reported values [12]. The calculated formation energies (E_f) are −4.12 eV and −3.83 eV for GaS and MD4 configuration at average lattice constant 3.42 Å respectively. The negative E_f values suggest their high stability and increased possibility of their successful synthesis in lab through experiments. It is also demonstrated that GaS and Zr_2CO_2 (MD4) has negative formation energies under biaxial

strain. The observed trend is in line with the earlier reported trend for the termination groups of atom or molecule such as $-O$, $-F$, and $-OH$ in functionalized Zr2C compounds [7]. It is experimentally observed that the formation energy of a compound increased with functionalization or applying pressure. Interestingly, the predicted trend of our results is in line with available experimental results.

We have addressed the structural, electronic, and thermoelectric properties of Zr_2CO_2 monolayers using PBE exchange-correction energy functionals [18]. In this article, we mainly focus on how the structural, and electronic properties change by stacking these different configurations of Zr_2CO_2 monolayers on GaS monolayers [(see Figure SI1(c,d)] using hybrid functional calculations. This led us to the investigation of eight stacking arrangements for Zr_2CO_2/GaS vdW hetero-structures: Zr_2CO_2 monolayers of varying configurations stacked on a GaS monolayer (referenced as rotational angle $\phi = 0^o$) [see Figure 1(a-h)]. The substrate GaS monolayer is rotated by $\phi = 180^o$ with respect to Zr_2 CO_2 monolayers, and further four possible stacking configurations of Zr_2 CO_2/GaS vdW heterostructures were considered [see Figure 2(a-h)].
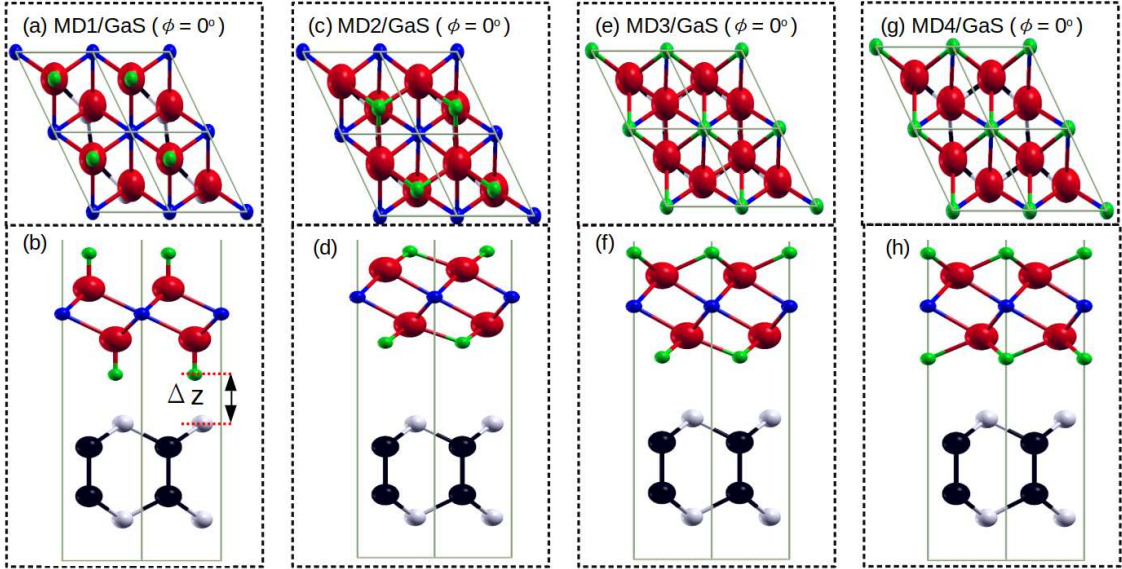

Figure 1: Schematic representations of top-view (upper panel) and side-view (bottom panel) of a conventional super-cell with dimensions $2 \times 2 \times 1$ of Zr_2CO_2/GaS vdW hetero structures in four realizable configurations: (a, b) MD1/GaS ($\phi = 0^o$), (c, d) MD2/GaS ($\phi = 0^o$) (e, f) MD3/GaS ($\phi = 0^o$) (g, h) MD4/GaS ($\phi = 0^o$). Zr, C, O, Ga and S atoms are represented by red, blue, green, black and white colors spheres, respectively.

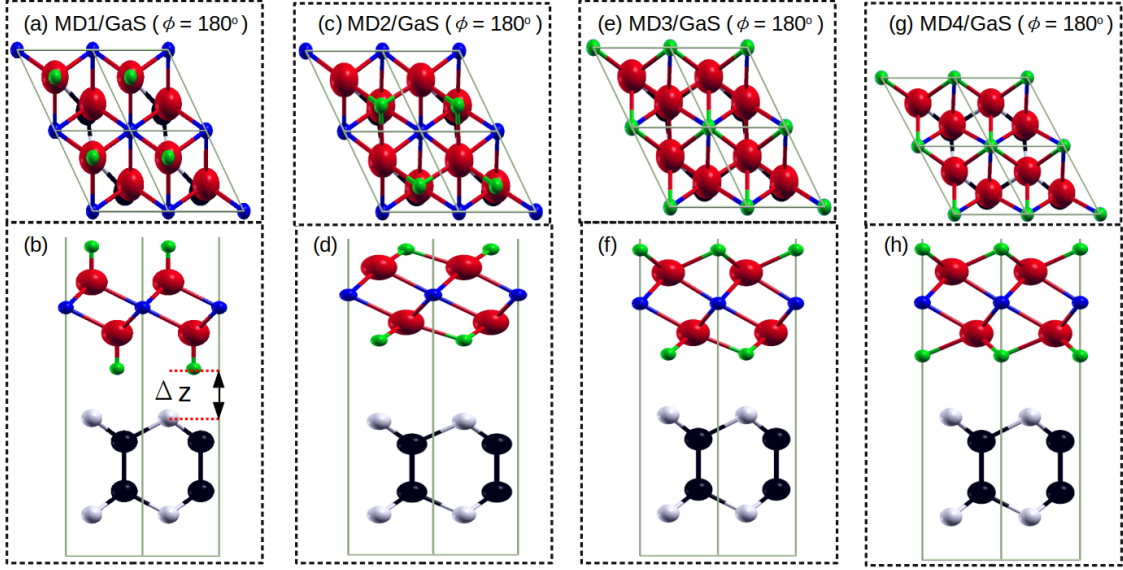Before considering the Zr_2CO_2/GaS vdW heterostructures, we analyzed the isolated GaS and

Figure 2: The substrate GaS monolayer rotated by $\phi = 180^o$ with respect to upper layer. So again there are four possible configurations. The schematic representations of top-view (upper panel) and side-view (bottom panel) of Zr_2CO_2/GaS vdW hetero structures are: (a, b) MD1/GaS ($\phi = 180^o$), (c, d) MD2/GaS ($\phi = 180^o$) (e, f) MD3/GaS ($\phi = 180^o$) (g, h) MD4/GaS ($\phi = 180^o$). Zr, C, O, Ga and S atoms are represented by red, blue, green, black and white colors spheres, respectively.

Zr_2CO_2 monlayers using GGA and HSE calculations. The results are summarized in Table I. The computed lattice constants for GaS and Zr_2CO_2 monlayers are 3.59 Å and 3.25 Å respectively, which are in agreement with previous works [18, 22]. Table I displays the GGA calculated optimized bond lengths, thickness (h) and bond angle θ which is in perfect agreement with the data from existing tests and theoretical predictions. For GaS and $Zr_2\ CO_2$ monlayers, the calculated E_f at equilibrium lattice constant are -8.27 eV and -8.77 eV, respectively. The negative formation energy confirms the thermodynamic stability of the GaS and $Zr_2\ CO_2$ monlayers. It is generally known that GGA-PBE calculations significantly underestimate the band gap of semiconductors. The Heyd-Scuseria-Ernzerhof (HSE06) method is, therefore, typically used to accurately estimate the bandgap.

The electronic structures of Zr_2CO_2 [see Figure 3(a-c)], GaS [see Figure 4(a-c)] were computed using the optimized lattice parameters. The GaS- and Zr_2CO_2 monolayer have HCP crystal structure belong to similar reciprocal lattice which has high symmetry k-points Γ, M, K, and Γ along the closed path in the first Brillouin zone (BZ). By considering these k-points, we investigated the

Table I: The calculated structural and electronic properties of GaS monolayer and Zr_2CO_2 monolayer (MD4 configuration) [18]. The optimized lattice constant, Ga-S, Zr-C, Zr-O bond lengths, and the height of the monolayer are denoted by a, b_{Zr-C}, b_{Ga-S}, b_{Zr-C}, b_{Zr-O}, and h, respectively. The θ denotes the bond angle between S-Ga-Ga and Zr-C-Zr atoms in GaS and Zr_2CO_2 monolayers, respectively. formation energies (denoted as E_f), bandgap calculated using GGA [HSE] energy functional denoted is denoted by E_g(GGA) [E_g(HSE)]. Here, we also listed the structural properties and electronic bandgap for of Zr_2CO_2 monolayer and GaS monolayers at the average lattice constant ∼3.42 Å to do comparison with Zr_2CO_2/GaS vdw Waals heterostructures in next section.

Sample	a	b_{Ga-S}	b_{Zr-C}	b_{Zr-O}	h	θ	E_f	E_g(GGA)	E_g(HSE)
	(Å)	(Å)	(Å)	(Å)	(Å)	degree	(eV)	(eV)	(meV)
GaS	3.59	2.34	-	-	4.61	120.16	−8.27	2.54	3.32
GaS	3.42	2.31	-	-	4.75	120.46	−4.12	2.72	3.49
MD4	3.25	-	1.75	2.51	4.26	83.9	−8.77	1.06	2.28
MD4	3.42	-	1.80	2.53	4.53	93.9	−2.83	1.31	2.78

electronic band structure, total density of state (TDOS) and partial density of states (PDOS) of the GaS and Zr_2CO_2 monolayer. The structural and electronic parameters are presented in Table I. The predicted band gaps for GaS and $Zr_2 CO_2$ monolayers using GGA+PBE (HSE) energy functional are 2.54 eV (3.32 eV) and 1.02 eV (2.28 eV), respectively, and are in good agreement with earlier theoretical works [18, 22, 42–44]. We also calculated the electronic properties for isolated GaS and $Zr_2 CO_2$ monolayers at optimal lattice constant as shown in the Figure SI3(a-c) and Figure SI4(a-c). Table I indicates that at the optimal lattice constant the bandgap for GaS ($Zr_2 CO_2$) monolayer increased to 3.49 eV (2.78 eV) consistent with previous works [18, 45].

Corresponding TDOS and PDOS of the HSE calculated bandstructure for Zr_2CO_2 monolayers (MD4 configuration) at ambient condition are presented in Figure 3(a-c). Figure 3(a) shows Zr_2CO_2 monolayers as a semiconductor with an indirect (Γ-M) bandgap. The semiconducting behavior of Zr_2CO_2 monolayers in MD4 configuration is further validate by total density of states as shown in the Figure 3(b). Furthermore, Figure 3(c) shows PDOS indicating VBM preeminent by d-orbital of zirconium atom and p-orbital of the carbon atoms. On the other hand, the CBM preeminently immersed by the d-orbitals of Zr atom and minor contribution from p-orbitals of

both carbon and oxygen atoms. The electronic bandgap of 0.98 eV for Zr_2CO_2 monolayer was calculated using GGA+PBE functional in the Ref [12]. While employing the most accurate most expansive GW method the estimated band gap of Zr_2CO_2 mnolayer is 2.26 eV [46]. As we know, GGA devalues the electronic bandgap [46], so the bandgap calculated by GGA is smaller than the value of bandgap calculated by GW. The quasi-particle bandgap of Zr_2CO_2 monolayers was predicted to be 2.13 eV [47].

Figure 4(a-c) presents the electronic bandstructure, TDOS and PDOS of GaS monolayer at ambient condition calculated using HSE functional. Figure 4(a) demonstrates that single layer GaS is a semiconductor with bandgap of value 3.32 eV (K-Γ), which is consistent with the previously calculated results [22]. Figure 4(b) shows the total density of state (TDOS) that confirms the semiconducting nature of GaS monolayer. Figure 4(c) shows the projected density of states (PDOS), which indicates that the CBM is located at Γ points while VBM is located in between M - Γ points. The VBM is mainly dominated by the p-orbitals of S atoms, while CBM is contributed by the p-orbital of Ga and S atoms [see Figure 4(c)]. Table I indicates that under applied biaxial strain the bandgap of Zr_2CO_2 (GaS) monolayer got decreased (increased) at average lattice constant. So it is also previously demonstrated that two-dimensional layered materials respond very well to applied biaxial strain [22].

From the above established discussion, we concluded that Zr_2CO_2 is stable in all possible configuration, so Zr_2CO_2 in MD4 configuration [see Figure SI1(a, b)] is investigated in further calculation.

B. Zr_2CO_2/GaS vdW heterostructures

Demirci et $al,$. showed that all group III-VI binary monolayers (GaS, GaSe, etc) have hexagonal crystal structures and are thermodynamically stable [48]. And Khan et $al,$ [43] demonstrated the dynamical stability of MXene monolayers upto 8 % applied biaxial strain. The GaS and Zr_2CO_2 monolayers have a lattice mismatch of 7.79 %, thus, it is suitable for creating Zr_2CO_2/GaS vdW heterostructures. For heterostructures structural optimization We initiated our calculations using the mean value of the lattice parameters of isolated monolayer. Adopting a 2×1 supercell model of Zr_2CO_2/GaS vdW heterostructures [see Figure 1(a-h) - Figure 2(a-h)]. Eight distinct types of stacking configurations were taken into consideration for the Zr_2CO_2/GaS vdW heterostructure, as shown in Figures 1(a-h) and Figure 2(a-h). Figure 1(a) illustrates a configuration known as Zr_2CO_2(MD4)/GaS $\phi = 0^o$, in which the zirconium atom is positioned above the sulfur atom and
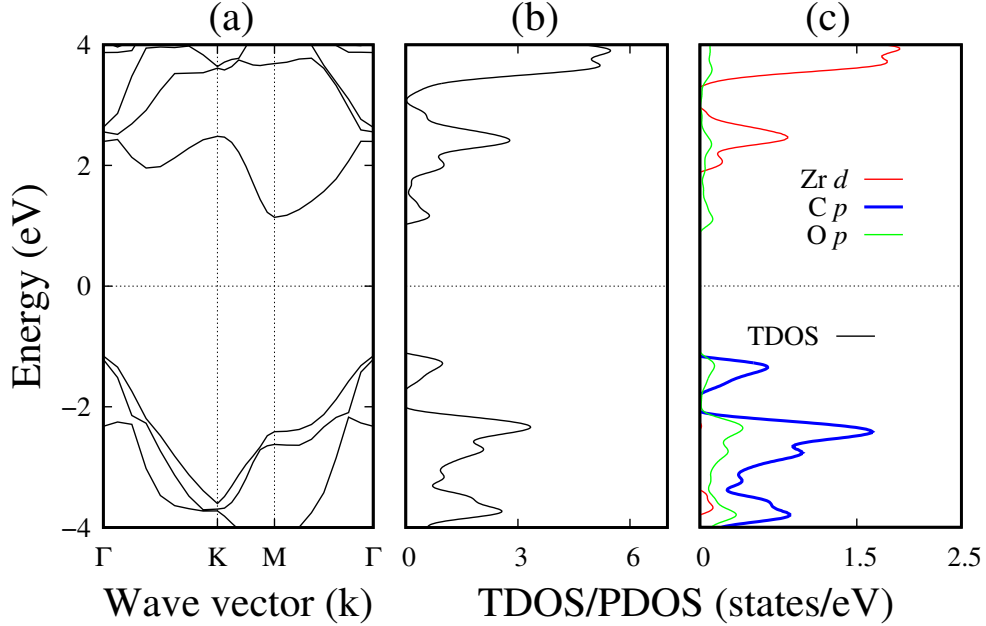
Figure 3: The electronic band structure TDOS amd PDOS of Zr_2CO_2 monolayer (MD4-configuration) calculated using HSE energy functional, (a) electronic band structure (b)TDOS, and (c) PDOS of Zr d-orbital, C and O atoms p-orbital are represented by red, blue and green color lines. The Fermi energy level is indicated by black dotted horizontal line.

the carbon atom is positioned above the gallium atom at the interface. Similarly, Figure 2(a) depicts the Zr_2CO_2 (MD4)/GaS $\phi = 180^o$) configuration, where the order of the atoms switches by 180 degrees at the interface. In this configuration, Zr lies above the Ga atom and the C lies above the S at the interface. We carried out the lattice constant optimization for all possible vdw Waals heterostructures, preserve the vacuum-slab constant along the z-axis. The optimized lattice parameter are 3.42 Å [see Figure SI2] and 3.38 Å for Zr_2CO_2 (MD4)/GaS $\phi = 0^o$ and Zr_2CO_2 (MD4)/GaS $\phi = 180^o$ configurations, respectively. We determined the relative adhesion energy, which is a measure of structural stability, and it is defined as

$$E_{ad} = E_{\text{tot}[Zr_2CO_2/GaS]} - E_{\text{tot}[Zr_2CO_2]} - E_{\text{tot}[GaS]} \tag{10}$$

where $E_{\text{tot}[Zr_2CO_2/GaS]}$ is the total electronic energy of Zr_2CO_2/GaS vdW heterostructure, and $E_{\text{tot}[Zr_2CO_2]}$ ($E_{\text{tot}[GaS]}$) is the ground state energy of single layer at ambient conditions lattice constant. The calculated relative adhesion energy (E_{ad} is negative which suggested that all vdW heterostructure are stable. The calculated relative adhesion energies are -6.57 eV and -6.48 eV for MD4/GaS $\phi = 0^o$ and MD4/GaS $\phi = 180^o$ vdw hetrostructures, respectively. The structural and electronic properties of Zr_2CO_2/GaS vdW heterostructures depend on the Zr_2CO_2 configurations.
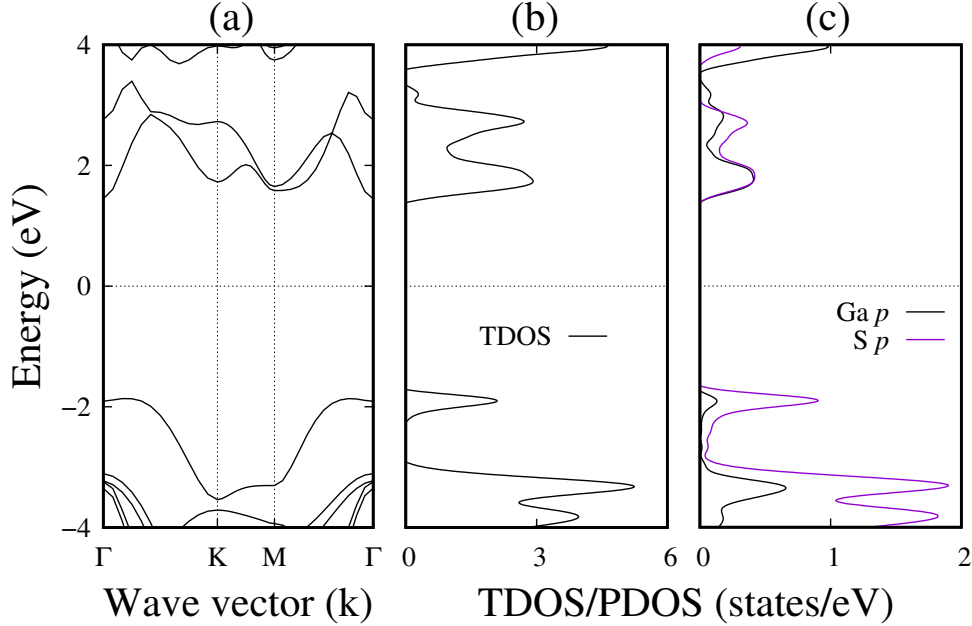
12

Figure 4: The electronic band structure TDOS amd PDOS of GaS monolayer calculated using HSE energy functional, (a) electronic band structure which shows that GaS is direct bandgap is $E_g = 3.30$ eV (Γ - Γ) (b)TDOS (c) PDOS of Ga p-orbital and S atoms p-orbital are represented by black and purple color lines. The Fermi energy level is indicated by black dotted horizontal line.

So, a systematic investigation of all possible Zr_2CO_2/GaS vdW heterostructures is waranted and relative adhesion energy will be calculated to investigate the structural stability.

The MXene/MoS$_2$ heterostructure was synthesized experimentally [49]. Researchers realized that by stacking different two-dimensional materials on top of each other, the vdW heterostructure is formed with tailored electronic properties as compared the isolated monolayers. Due to weak vdW bonding between layers of vdw heterostructure, the electronic properties tuned around the electronic properties of isolated monolayers. This tunability is crucial for constructing new devices with specific functionalities. Excellent electronic character induces only at the interface, e.g some two dimensional materials have high conductivity. So,stacking them in vdw heterostructure can results in excellent charge transport across the interface. Besides these, the interlayer interaction plays an important role, that can generate new excitonic states, which results in an enhanced photon-matter interactions. At first glance, we did optimization for the GaS and Zr2CO2 monolayers and then designed the Zr_2CO_2/GaS vdW heterostructure at the mean value of the lattice parameters of the 2D materials.

Table II: Adhesion energy (E_{ad}) and relative energy ΔE with reference to the most stable configuration, interlayer distance Δz_{SO} (vertical distance between the bottom oxygen atom of the Zr_2CO_2 monolayer and the top chalcogen atom of the GaS monolayer), GGA calculated bandgap is denoted by $E_g(GGA)$ and HSE calculated bandgaps is denoted by $E_g(HSE)$ of the possible configurations considered for the Zr_2CO_2/GaS vdW heterostructures [see Figure 1(a-h) - Figure 2(a-h)]]. For the inplane dimensions of the Zr_2CO_2/GaS vdW heterostructures, we simulated the supercell with the approximate average value of the lattice constants of isolated monolayers.

configuration	E_{ad} (eV)	ΔE (meV)	Δz_{S-O} (Å)	$E_g(GGA)$ (eV)	$E_g(HSE)$ (eV)
MD1/GaS					
(a) Zr_2CO_2/GaS ($\phi = 0^o$)	−6.40	159.25	4.18	1.21	2.34
(b) Zr_2CO_2/GaS ($\phi = 180^o$)	−6.48	89.02	4.12	1.19	2.31
MD2/GaS					
(a) Zr_2CO_2/GaS ($\phi = 0^o$)	−6.45	122.28	4.19	1.22	2.19
(b) Zr_2CO_2/GaS ($\phi = 180^o$)	−6.44	125.98	4.19	1.22	2.19
MD3/GaS					
(a) Zr_2CO_2/GaS ($\phi = 0^o$)	−5.51	1060.3	2.67	1.15	2.01
(b) Zr_2CO_2/GaS ($\phi = 180^o$)	−5.79	777.08	2.60	0.45	1.15
MD4/GaS					
(a) Zr_2CO_2/GaS ($\phi = 0^o$)	−6.57	0.0	2.63	0.98	2.18
(b) Zr_2CO_2/GaS ($\phi = 180^o$)	−6.48	88.21	3.17	1.21	2.60

Table II shows that all possible Zr_2CO_2/GaS vdW heterostructurs have negative adhesion energies, which confirm the structural stability. The negative adhesion energy indicates the Zr_2CO_2 has attractive interaction with the GaS monolayer via vdW force. For example, being considered the most stable MD4/GaS vdW heterostructure $\phi = 0^o$, the calculated relative adhesion energy E_{ad} for the fully relaxed Zr_2CO_2/GaS vdW heterostructure is smaller than the E_f of the Zr_2CO_2 monolayer, which confirms the structural stability of Zr_2CO_2/GaS heterostructure. Our findings are comparable with earlier reported values of $E_{ad} = -39.9$ meV/per-atomic-pair for the C_2N/Zr_2CO_2 vdw Waals heterostructure [50]. Also, another reported value of E_{ad} is -33.4 meV/per-atomic-pair

for the vad Waals heterostructur of Zr_2CO_2 and InSe monolayers [46]. Consequently, all designed Zr_2CO_2/GaS vdW heterostructures are thermodynamically stable and can be synthesized experimentally. The $\Delta z_{SO})$ defined interlayer interacting distance i.e the vertical distance between the bottom oxygen atom of the Zr_2CO_2 monolayer and the top chalcogen atom of the GaS monolayer. The calculated Δz_{SO} are 2.63 Å 3.17 Å for MD4/GaS vdW heterostructure at $\phi =0^o$ and $\phi =180^o$ configurations, adhere with relative adhesion energy. The Δz_{SO} values got smaller in the most favorable vdw heterostructure [see Table II.

To correctly understand the vdW interaction mechanism between two dimensional stacking materials, the electronic band structure of the Zr_2CO_2 (MD4)/GaS vdW heterostructure are further explored. The calculated GGA (HSE) electronic bandgap is 0.98 eV (2.18 eV) for MD4/GaS configurations at $\phi =0^o$. Furthermore, for Zr_2CO_2 (MD4)/GaS $\phi =180^o$ vdw Waals heterostructure, the GGA (HSE) calculated electronic bandgap is 1.21 eV (2.60 eV). Due to the exceptional sensitivity to mechanical strain of 2D materials, the modest variation in the electronic bandgap occurred [22]. Because, when a 2D layered material is subjected to biaxial strain its atomic positions altered, which results in tailored electronic properties. The GGA+PBE calculated electronic band structures for all possible configurations are presented in Figure SI5(a-c) - Figure SI7(a-c).

Figure 5(a-c) shows the calculated band structure, TDOS and PDOS of MD4/GaS vdW heterostructure for configurations $\phi = 0^o$. Figure 5(a) shows MD4/GaS is an indirect bandgap semiconductor. The indirect and direct bandgaps are 2.18 eV (Γ-K) and 3.20 eV (Γ-Γ), respectively. For Zr_2CO_2/GaS ($\phi = 0^o$) the conduction band maximum and valance band minimum are laying at Γ and K point of the first brillouin-zone, respectively. Similarly, the combination of Zr_2CO_2 and $MoSe_2$ in a vdw Waals heterostructure with an indirect bandgap of amount 0.79 eV (Γ-M) consisting with our work, and suggests interesting material for optoelectronic application [12]. Figure 5(b) presents the total density of state which validate the bandgap of Zr_2CO_2/GaS ($\phi = 0^o$) vdW heterostructure. Figure 5(c) shows the partial density of state, which shows the carbon atom p-orbitals has prominant contribution to the valance band edge. In comparison, conduction band edge is dominated by the hybridization of zirconium atom d-shell with a small sharing of gallium, sulfur p-shell. It should be noticed that valance band edge is primarily formed by a Zr_2CO_2 monolayer, in comparison to an isolated Zr_2CO_2 monolayer with an indirect bandgap of 1.3 eV (Γ-M) [see Figure 3(a)] and isolated GaS single layer with an indirect bandgap of value 3.32 eV (Γ - K) [see Figure 4(a)].

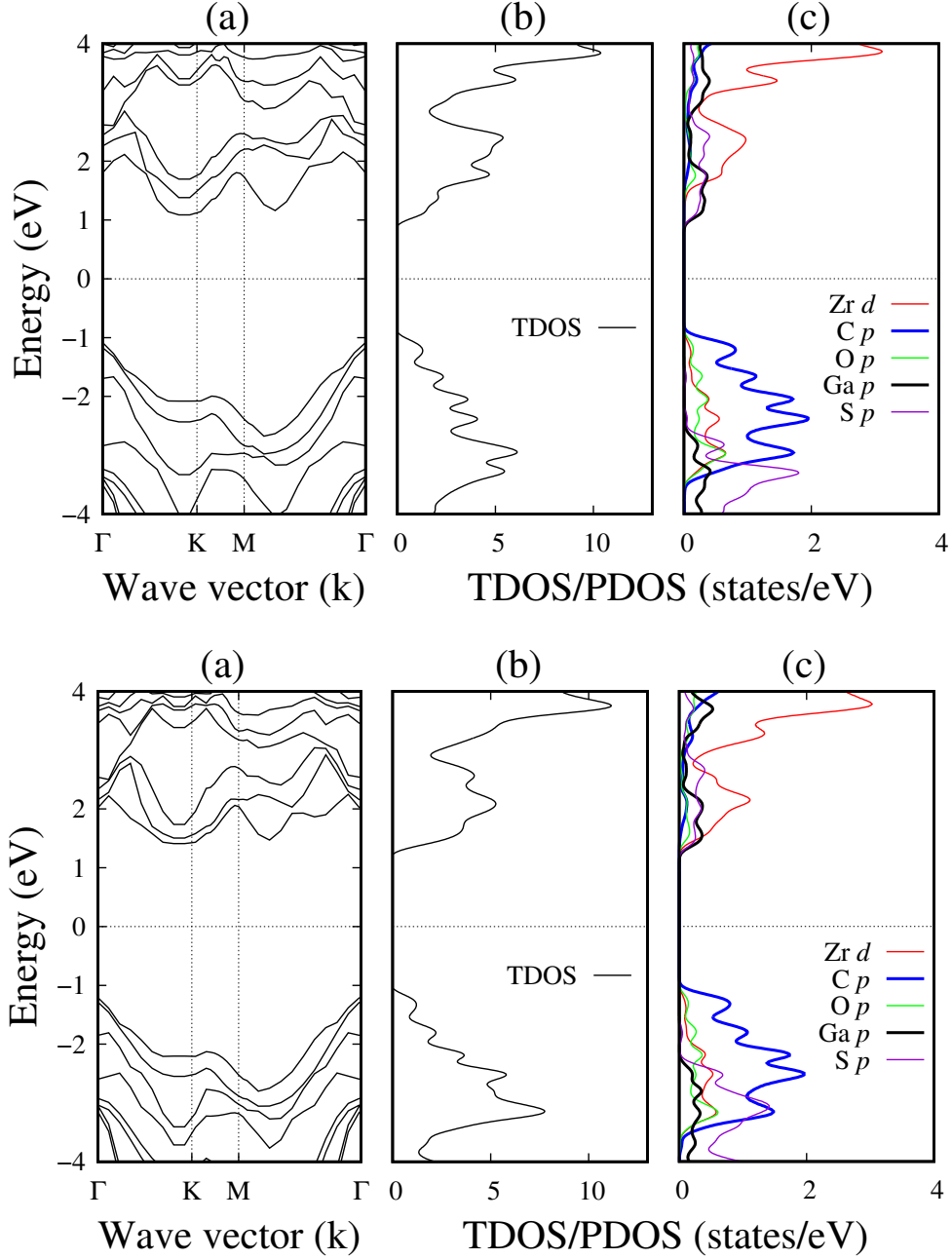It is noted that the CBM is displaced to the K point as a result of heterostructur formation

Figure 5: The electronic band structure TDOS amd PDOS of MD4/GaS vdW heterostructures calculated using HSE energy functional at different stacking angle top one has $\phi = 0^o$) and bottom one has $\phi = 180^o$, (a) electronic band structure (b)TDOS and (c) PDOS of Zr atom d-orbital, C, O , Ga, and S atoms p-orbitals are represented by red, blue, green, black and purple color lines. The Fermi energy level is indicated by black dotted horizontal line.

as shown in Figure 5(a)(top and bottom). Note that due to Zr_2CO_2 (MD4)/GaS heterostructure formation the bandgap value increased (decreased) by 0.88 eV (1.14 eV) as compared with Zr_2CO_2 (GaS) monolayer. These finding can be explained by the band offset of solitary monolay-

ers. Furthermore, the interlayer vdw interaction results in larger bandgap of Zr_2CO_2 MD4/GaS vdW heterostructure as comapred to solitary Zr_2CO_2 monolayer [51], similar finding were reported for BP/MoS_2 vdw heterostructure [52]. Staking of different 2D materials results in reduced lattice parameter a_o (see Figure SI2), i.e, the relaxed crystal structure of the heterostructure has minimum ground state energy at approximately average lattice constant of the constituent monolayers. Reduction in the bond length, or lattice constant induces an enhanced bandgap of the Zr_2CO_2 (MD4) monolayer laying in the visible range of solar spectrum and adhere with our previously reported work [22, 53, 54]. Two-dimensional materials with moderate bandgap are required for optoelectronic devices. Looking at the earlier work on both Zr_2CO_2 and GaS monolayer, and Zr_2CO_2/GaS vdw Waals heterostructure from the perspective of the optical applications, we determined that exhaustive investigation of the electrical and optical response of the Zr_2CO_2/GaS vdw Waals heterostructures in the visible range of the solar spectrum is warranted. And covering the visible range of solar spectrum are still lacking to the best of our knowledge. In this regards, the detail optical characteristics of Zr_2CO_2, GaS monolayers, and Zr_2CO_2/GaS vdW heterostructure in most stable configuration have been considered for further investigations.

C. Optical properties

We adopted GGA functionals and HSE functional that provide improvement over GGA results and investigated the optical characteristics. The real part $\epsilon_1(omega)$ of the dielectric function which depends upon of incident photon energies are calculated for GaS-, Zr2CO2-, and MD4/GaS $\phi = 0^o$ vdW heterostructures [see Figure 6(a, b)]. The electronic polarizability is the basic property of an atom, molecules or material which define how the atoms or molecules or material respond to external electric field. So, the real part $\epsilon_1(\omega)$ impart the knowledge about the response of a material to electric field known as electric polarizability. The statics value of $\epsilon_1(\omega)$ is calculated by considering the limit on frequency approaches to zero [55]. Using GGA functional $\epsilon_1(\omega = 0)$ for GaS-, Zr_2CO_2-monolayer, and Zr_2CO_2/GaS vdW heterostructures are 4.08, 5.82, and 6.25, respectively. Figure 6(a) shows that the $\epsilon_1(\omega)$ plots calculated by GGA reached maximum values of 7.75, 13.91, and 9.93 at energies of 3.5 eV, 1.03 eV, and 2.03 eV for GaS-, Zr_2CO_2-monolayers, and Zr_2CO_2/GaS vdW heterostructure. Similarly, Figure 6(b) presented the $\epsilon_1(omega)$ plots calculated by HSE functional, which attained their maximum values of 4.83, 7.18, and 6.13 at energies of 4.32 eV, 3.03 eV, and 6.13 eV for GaS-, Zr_2CO_2-monolayers, and Zr_2CO_2/GaS vdW heterostructure, respectively. Both GGA and HSE calculations indicate that there exists a small

energy interval (2 eV − 4) in which the real part $\epsilon_1(omega)$ has adverse polarization indicated by negative value of $\epsilon_1(omega)$. This demonstrates the conducting nature of the Zr_2CO_2 monolayer.
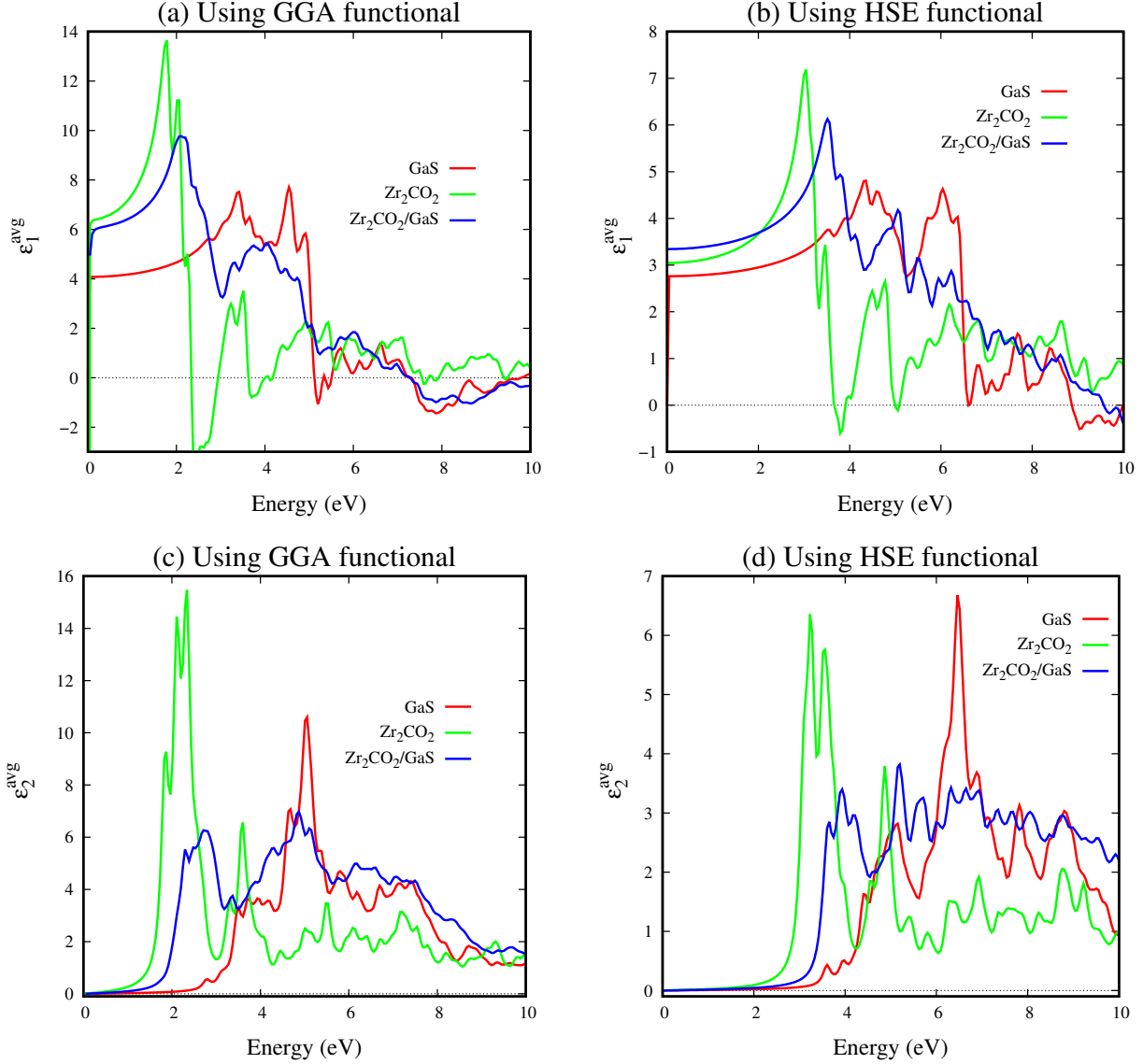

Figure 6: The optical spectra of a GaS monolayer and a Zr_2CO_2 monolayer are computed at their equilibrium lattice constants, while for the MD4/GaS $\phi = 0^\circ$ vdW heterostructure, the optical spectra is calculated at the approximate average lattice constant of isolated monolayers. The real part of the dielectric function is calculated (a) using the GGA energy functional and (b) using the HSE energy functional. The imaginary part of the dielectric function is calculated (c) using the GGA energy functional and (d) using the HSE energy functional, The red, green, and blue lines show the calculated spectra of a pure GaS monolayer, a pure Zr_2CO_2 monolayer, and a MD4/GaS vdW heterostructure, respectively.

The second part of the dielectric function $\epsilon_2(\omega)$ is a tensor and it has three non-zero components,

which are $\epsilon^{xx}(\omega)$, $\epsilon^{yy}(\omega)$, and $\epsilon^{zz}(\omega)$. To reduce error in our simulated results, we take average of all these three tensor parts of $\epsilon_2(\omega)$. The $(\epsilon_2(\omega))$ depends upon the incident photon energy and calculated for GaS-, Zr_2CO_2-monolayers, and Zr_2CO_2/GaS vdW heterostructures employing GGA and HSE functionals [see Figure 6(c, d)]. The $\epsilon_2(\omega)$ describe the real electron transitions between the occupied and unoccupied states. Figure 6(c) indicates that $\epsilon_2(\omega)$ under 1.0 eV, 1.3 eV, and 2.54 eV is nearly zero because of the forbidden electronic transitions between valance band maximum (VBM) and conduction band minimum (CBM) for GaS-, Zr_2CO_2-monolayers and Zr_2CO_2/GaS vdW heterostructure, respectively. From $\epsilon_2(\omega)$, we can extract details about the samples' bandgap and absorption characteristics [55]. The curves of the $\epsilon_2(\omega)$ initiated abrupt increase as the incident em-waves energies got comparable to their electronic band gap listed in Table I and Table II. The GGA-calculated $(epsilon_2(\omega)$ is shown in Figure 6(c), which follows the same trend as the HSE function (see Figure 6(d)). For example, Figure 6(c) indicates that $\epsilon_2(\omega)$ plots calculated by GGA start absorption of photon energy at 2.54 eV, 0.81 eV and 1.2 eV, for GaS-, Zr_2CO_2-monolayers and Zr_2CO_2/GaS vdW heterostructure, respectively. Similarly, the $epsilon_2(\omega)$ plots calculated by HSE functional start absorption of photon energy at 3.32 eV, 1.3 eV, and 2.1 eV for GaS, Zr_2CO_2-monolayers, and Zr_2CO_2/GaS vdW heterostructure. These absorption peaks are produced in a GaS-monolayer due to the transition of electrons from S-p state to Ga-p state. In the case of Zr_2CO_2-monolayers, these peaks are caused by electron transitions from the C-p to the Zr-d states. Absorption peaks are produced in Zr_2CO_2/GaS vdW due to an electron transition from the C-p state to the Ga-p state. Figure 1 top figure, indicates that electrons are localized in different monolayers, and fulfill the definition of the type-II heterostructure, which is required for solar-cell applications. The numerous peaks are observed ahead the first peak of $\epsilon_2(\omega)$ spectrum of the isolated GaS-, and Zr_2CO_2-monolayers, as shown in Figure 6(c, d).
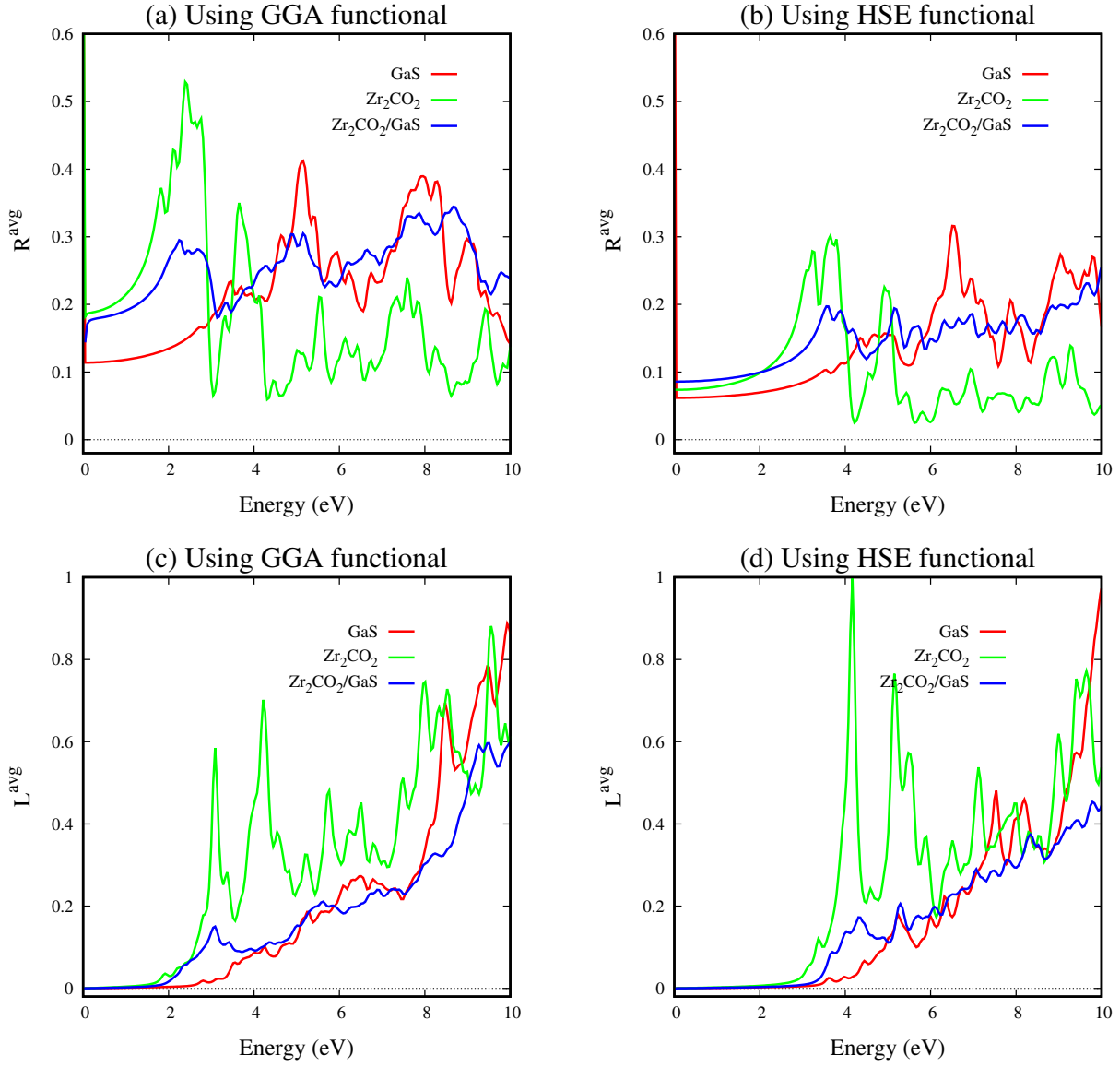
Figure 7: At the equilibrium lattice constant of isolating monolayers, the reflectivity is calculated (a) using the GGA energy functional and (b) using the HSE energy functional for GaS monolayer and Zr_2CO_2 monolayer, while for the MD4/GaS $\phi = 0^\circ$ vdW heterostructure, we used the average lattice constant for calculations. The electron energy loss is computed (c) using the GGA energy functional and (d) using the HSE energy functional. The red, green, and blue lines show the calculated spectra of a pristine GaS monolayer, a pristine Zr_2CO_2 monolayer, and a MD4/GaS $\phi = 0^\circ$ vdW heterostructure, respectively.

Figure 7(a, b) shows the calculated reflectivity as a function of photon energy using (a) GGA and (b) HSE functional calculations. The GGA calculated reflectivity at zero frequency limit is found to be 11 % and 18 % and 19 % for GaS- and Zr_2CO_2-monolayers, and Zr_2CO_2/GaS

vdW heterostructure, respectively. Similarly, using HSE functional reflectivity calculated at zero frequency limit is found to be 6.19 % and 7.5 % and 8.61 % for GaS- and Zr_2CO_2-monolayers, and Zr_2CO_2/GaS vdW heterostructure, respectively as tabulated in Table II. The limiting values of HSE calculated reflectivity are obtained to be 31.0 % at 6.5 eV, 30.0 % at 3.64 eV and 19.22 % at 3.57 eV, for GaS- Zr_2CO_2-monolayers, and Zr_2CO_2/GaS vdW heterostructures, respectively. This indicate that first peak shifted to lower wavelength and blue shift occurred due to heterostructure formations. The reflectivity fluctuates around 0.15 in the energy range of 3 eV to 10 eV for Zr_2CO_2/GaS vdW heterostructures. The fluctuation trend is opposite to that of the first peak change trend. Figure 7(c, d) presented the inelastic interaction of photon with electron in a material termed as electron energy loss (EEL) calculated with GGA and HSE functional. The electron energy loss spectrum is linked to the energy loss that happens when fast electrons moving through a material interact with each other because plasmons are excited. Inelastic scattering occurs when incident photon transfer fraction of its kinetic energy to the electron in the GaS-, Zr_2CO_2 monolayers, and Zr_2CO_2/GaS vdW heterostructures, which results in the increase of electron energy loss with variation of incident photon energy. This results in an increased probability of electron interaction as incident em-wave energy escalate from a limiting value upto 10 eV. Figure 7(d) indicates that HSE calculated electron energy loss spectra of Zr_2CO_2 has first peak at 3.0 ev and upon heterostructure formation it is shifted to 3.8 eV. So, the peak has red shift with the formation of Zr_2CO_2/GaS vdW heterostructures.

Table III: The optical characteristics namely; real part (ϵ_1) of the complex dielectric function, n, R, α calculated employing screened hybrid functional. The calculated zero (high) frequency limit values at first peak (denoted as: 1st-peak) and peak value of the absorption (α_{max}) are tabulated for GaS, Zr_2CO_2 monolayers and Zr_2CO_2/GaS ($\theta = 0^o$) vdW heterostructures.

Sample	$\epsilon_1(0)$	$\epsilon_1(max)$	n(0)	n(max)	R(0)	R(max)	$\alpha(\omega)$ 1st Peak	Maximum $\alpha(\omega)$
GaS	2.70	4.83	1.66	2.30	6.19 %	31.0 %	3.85	112.4
Zr_2CO_2	3.08	7.18	1.75	2.74	7.5 %	30.0 %	146.14	76.2
Zr_2CO_2/GaS ($\theta = 0^o$)	3.38	6.13	1.84	2.51	8.6 %	19.7 %	22.8	115.9

Employing generalized gradient approximation (GGA) and screened hybrid functional (HSE) the calculated variation of extinction coefficients as a function of incient photon energy of the GaS, Zr_2CO_2 monolayers, and Zr_2CO_2/GaS vdW heterostructure are presented in Figure 8(a, b). The extinction coefficient variation with respect energy follow the trend completely identical with that of the $\epsilon_2(\omega)$. Figure 8(c. d) presented the refractive index of all studied compounds
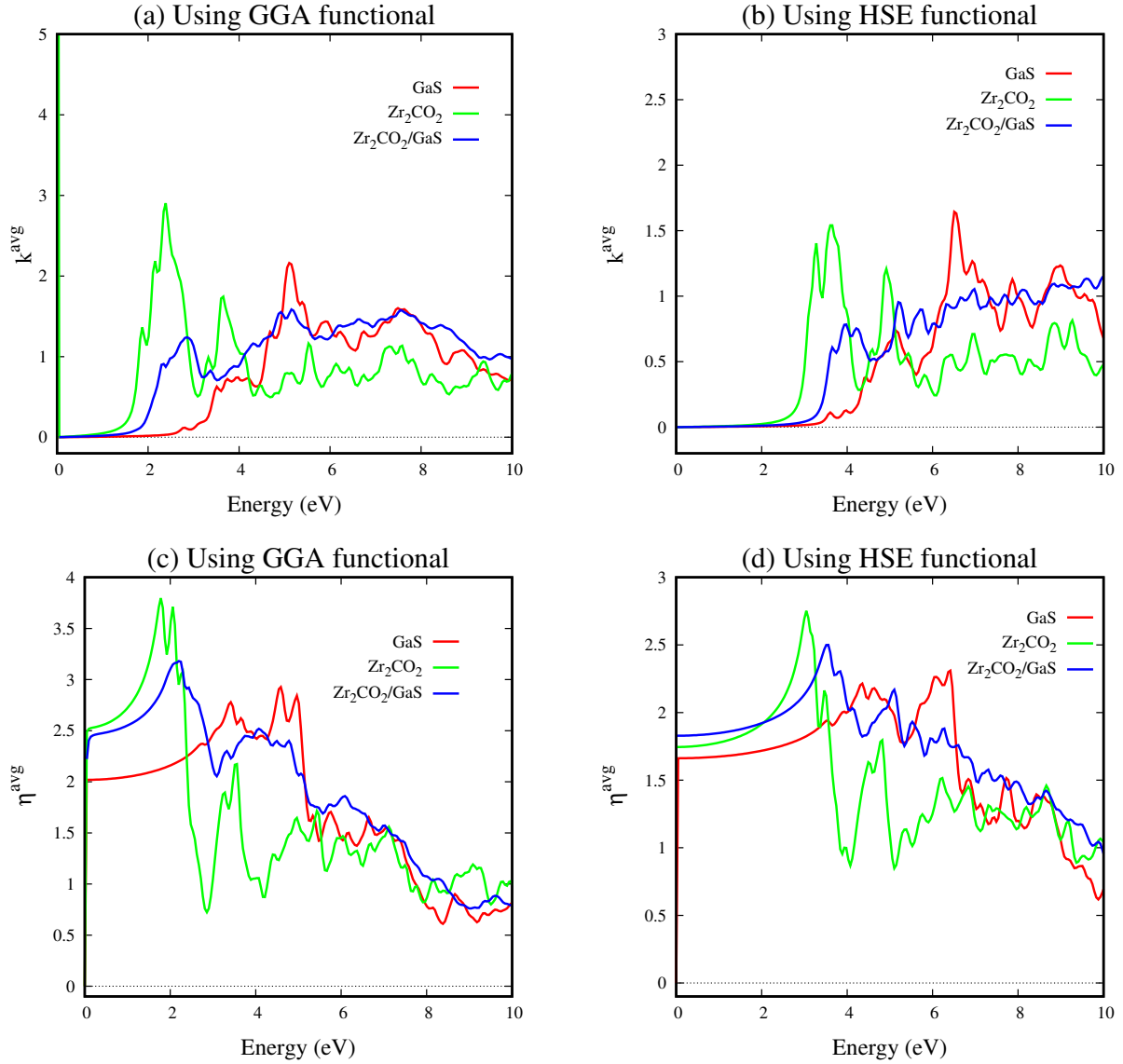
Figure 8: The optical spectra of a GaS monolayer and a Zr_2CO_2 monolayer are computed at their equilibrium lattice constants, while for the MD4/GaS $\phi = 0°$ vdW heterostructure, the optical spectra is calculated at the mean value of the lattice constants of isolated monolayers. The extinction coefficient is calculated (a) using the GGA energy functional, and (b) using the HSE energy functional. The refractive index is calculated (c) using the GGA energy functional, and (d) using the HSE energy functional, The red, green, and blue lines show the calculated spectra of a pure GaS monolayer, a pure Zr_2CO_2 monolayer, and a MD4/GaS $\phi = 0°$ vdW heterostructure, respectively.

under consideration as a function of electromagnetic wave "composed of photon" energy. The zero frequency values of refractive index are 1.45, 1.63 and 1.945 for GaS monolayer, a pure Zr_2CO_2 monolayer, and a Zr_2CO_2/GaS, respectively. As discussed earlier, The electron density

22

directly effect the optical characteristics, so electron density directly affected the refractive. The electron density increases as a result probability of photon−electrons interaction got enhanced, and maximum values of refractive index is achieved. As primitive cell volume of Zr_2CO_2 (74.08 Å^3) is smaller than that of GaS (109.21 Å^3), a higher value of refractive index is achieved for Zr_2CO_2 monolayer because Zr_2CO_2 monolayer has higher electron density then GaS monolayer. The calculated highest refractive index are 2.37 at 5.10 eV for Zr_2CO_2 monolayer, and 2.80 at 4.77 eV for GaS monolayer. An isolated GaS monolayer at low frequency behave like transparent materials, as evidenced by their low photon energy absorption and reflectivity. This is because the GaS monolayer's refractive index at lower frequencies is near to that of glass. Referring to it, the band gap gets smaller as the interface causes strain, which changes the optical properties. The absorption spectra show that the cutoff frequency in the Zr_2CO_2/GaS vdW heterostructure changes to a lower value as a result of the interface effect. So, these materials pass light until the optical band gap and shift happen at the threshold frequency. At the equilibrium lattice constant, Figure 8(b) shows the HSE calculated steady state refractive indices of the GaS monolayer, Zr_2CO_2 monolayer, and Zr_2CO_2/GaS vdW heterostructure are 1.66, 1.75, and 1.84, respectively.
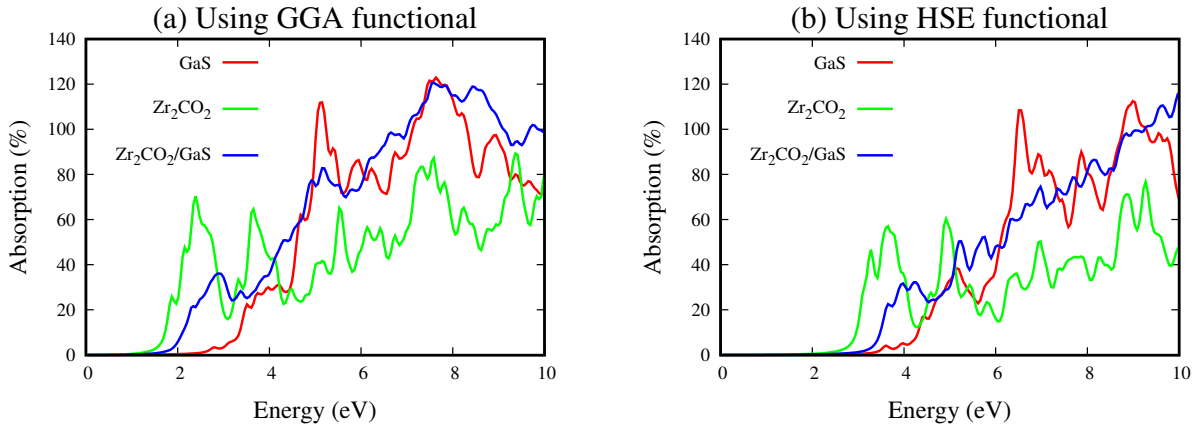

Figure 9: The absorption coefficients of a GaS monolayer and a Zr_2CO_2 monolayer are computed at their equilibrium lattice constants, while for the MD4/GaS $\phi = 0°$ vdW heterostructure, For crystal structure simulations the mean value of lattice parameters of the isolated monolayers is adopted. (a) using the GGA energy functional and (b) using the HSE energy functional. The red, green, and blue lines show the calculated absorption coefficients of a pure GaS monolayer, a pure Zr_2CO_2 monolayer, and a MD4/GaS $\phi = 0°$ vdW heterostructure, respectively.

Light absorption in two-dimensional compounds can be surprisingly more intense than in bulk materials [56]. It can be measured by the absorption coefficient, namely the fraction of light

absorbed at a given photon energy. Employing GGA+PBE functional and HSE functional the absorption coefficient of isolated monolayers, and a most stable Zr_2CO_2/GaS vdW heterostructure are investigated [see Figure 9(a, b)]. The absorption coefficient is calculated for the range of incident photon energies 0 eV$-$10 eV [see Figure 9(a, b)]. The absorption coefficient increasing trend is inline with electronic bandgap and $\epsilon_2(\omega)$. After limiting electronic band gap, absorption coefficients quickly increasing and maximum peak values is achieved at higher energies. The limiting energies values of GaS monolayer, pure Zr_2CO_2 monolayer, and a Zr_2CO_2/GaS vdW heterostructure are compared with electronic bandgap calculated using GGA. (see Table II). The GGA calculation show that the initial peak is occurred; at 4.0 eV for GaS, at 2.2 eV for Zr_2CO_2, and at 2.8 eV for Zr_2CO_2/GaS vdW heterostructure. This trend is followed by the HSE calculations. Figure 9(a) indicates the maximum values of GGA+PBE calculated absorption coefficients are 120.4 at 7.8 eV, 90.02 at 9.21 eV and 119.9 at 7.8 eV, for GaS monolayer, Zr_2CO_2 monolayer, and Zr_2CO_2/GaS vdW heterostructure, respectively. Figure 9(b) indicates HSE calculated absorption coefficients and the maximum values are 112.4 at 9.0 eV, 76.2 at 9.29 eV and 115.9 at 10.0 eV, for GaS monolayer, Zr_2CO_2 monolayer, and Zr_2CO_2/GaS vdW heterostructure, respectively.
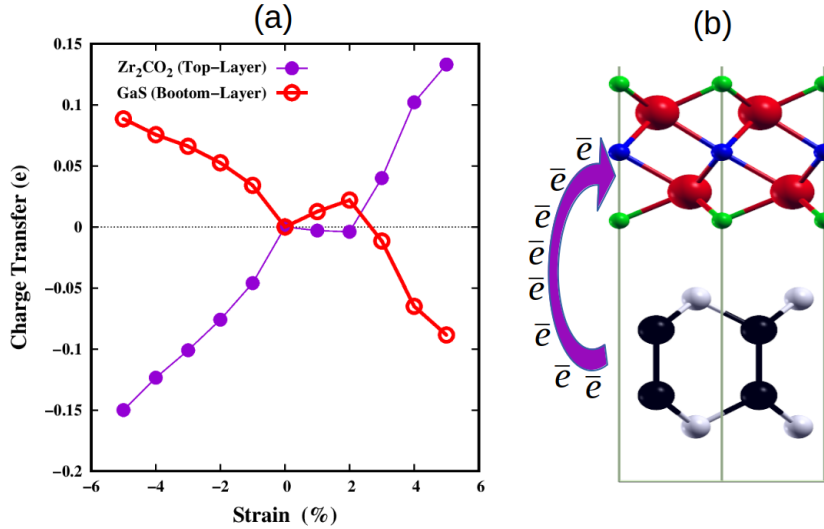
Figure 10: The charger transfer (CT) from bpttom layer to top layer in case of Zr_2CO_2/GaS ($\phi = 0^o$) vdW heterostructure under different bi-axial strain. The red line indicates the CT on GaS monolayer and megneta line indicates the CT on Zr_2CO_2 monolayer.

Figure 10(a,b) represent the schematic representation of charge transfer among the different layers of vdw Waals heterostructures. The CT value as a function of strain are found by calculating the total charge on layer with respect to the CT value on layer at $\epsilon = 0\%$. Figure 10(a) indicates

that GaS (Zr_2CO_2) monolayer losses (gained) fraction of charge under compressive bi-axial strain act as a donor (acceptor). While in the case of tensile strain the GaS (Zr_2CO_2) gained (losses) fraction of charges, so the stress-strain changes the amount of charge transfer of monolayers in a vdw Waals Heterostructures and alters the nature of electronic structure of materials.
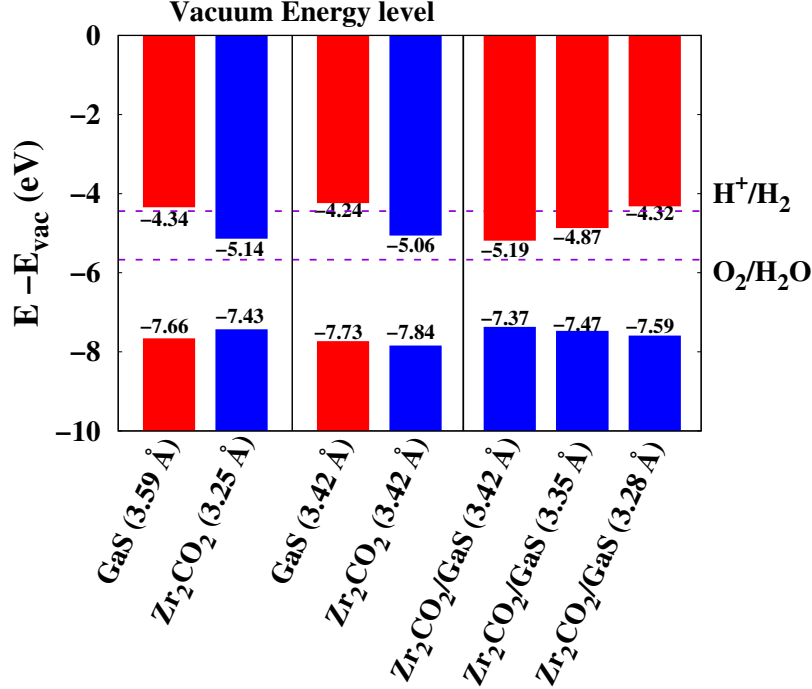

Figure 11: The band alignmnet of a GaS monolayer, a Zr_2CO_2 monolayer and MD4/GaS ($\phi = 0^o$) vdW heterostructure at different lattice constant, the VBM and CBM are calculated with respect to vacuum level. The red, and blue band show the calculated bands of a pure GaS monolayer, and pure Zr_2CO_2 monolayer, and a MD4/GaS vdW heterostructure, respectively. We considered three panel for band alignment, (i) pristine monolayer at their equilibrium lattice constant (Left panel), (ii) GaS and Zr_2CO_2 monolayers at average lattice constant (Middle panel), (iii) MD4/GaS ($\phi = 0^o$) vdW heterostructure (Right panel) at different lattice constants. The horizontal red dashed lines represents standard water redox potentials for H^+ and OH^- ions. The vacuum level at zero eV is set to reference potential.

The absorption coefficient and work function are concepts related to the interaction of electromagnetic radiation (such as light) with materials, specifically in the context of solid-state physics and material science. The relationship between the work function (Φ) and the absorption coefficient ( ) is not straightforward, as they are related to different physical phenomena. However, both are important concepts in understanding the interaction of light with materials and finding

25

applications in various fields, such as photovoltaics, photoemission spectroscopy, and optoelectronic devices. The minimum amount of energy required to eject the loosely bound electrons from the metal surface is known as work function (Φ). The work function of a material is required as reference for band alignment. Mathematically, it is define as

$\Phi = E_{vacuum} - E_F$ here E_{vacuum} and E_F are the vacuum and Fermi energy levels of the materials, respectively. Figure SI7(a-c) show the electrostatics potentials for GaS, Zr_2CO_2, and Zr_2CO_2/GaS vdW heterostructure, respectively.

Figure SI7(a-c) represent the calculated electrostatic potential for isolated monolayers and vdW heterostructure. The calculated Fermi energies for GaS, Zr_2CO_2 monolayers, and MD4/GaS $\phi = 0^o$ vdW heterostructures are -5.04 eV, -5.03 eV, and -4.57 eV, respectively, with respect to the vacuum energy level. To impels the photo generated electrons, we have calculated vacuum energy levels for GaS, Zr_2CO_2 monolayers, and MD4/GaS $\phi = 0^o$ vdW heterostructures are 5.81 eV, 6.30 eV, and 8.51 eV, respectively. Figure 11 presented band alignment of isolated monoilayers and Zr_2CO_2/GaS vdw heterostructure at equilibrium lattice constant and strained lattice constant. By looking at the projected density of states (PDOS) of the heterostructures, as shown in Figure 5 (top and bottom), we can see that in both heterostructures, the highest valence bands primarily come from the p-orbitals of the C atoms and CBM dominated by Ga p orbitals, the contribution from the Zr d-orbitals is minor. This shows that the MD4/GaS vdw heterostructures has a type-II band alignment, which is good for photovoltaic applications. The Zr_2CO_2/GaS vdW heterostructure forms type-II band alignment through which electron and holes can be separated in different layers. Such type of heterostructure have demanding applications in solar cell, and water splitting. Similar GGA+HSE calculation has been reported in Refs. [57, 58].

The redox potential for water splitting demands that the conduction band minimum (CBM) be more negative than the redox potential of H^+/H_2 and the valence band maximum (VBM) be more positive than the redox potential of O_2/H_2O [59]. For green energy applications, our findings suggest that a Zr_2CO_2/GaS van der Waals heterostructure is more promising for water splitting than an isolated monolayer because narrowing the band gaps would result in more excellent solar spectrum absorption; as Zhuang and Hennig demonstrated in Reference. [60], isolated Zr2CO2 and GaS monolayers have too large band gaps. In contrast, the formation of heterostructures is harmful to water splitting in Zr2CO2 and GaS because the VBM and CBM of the heterostructures are already too close to the H^+/H_2 redox potential [60], and the downward shift caused by heterostructure formation may bring the CBM below the H^+/H_2 potential. Zr_2CO_2/GaS van

der Waals heterostructure has type-II band alignment under 3% biaxial compressive strain, which meets the condition for photocatalytic water splitting, with the GaS (Zr_2CO_2) monolayer acting as an electron acceptor (donor). The Zr_2CO_2/GaS vdw Waals heterostructure meets the condition for photocatalytic water splitting, with the GaS (Zr_2CO_2) monolayer acting as an electron acceptor (donor). The electrons are transferred from Zr_2CO_2 monolayer to the GaS monolayer, resulting in the accumulation of electrons on the GaS side and holes on the Zr_2CO_2 side, which implies that a built-in electric-field is formed at the interface. This built-in electric-field would improve the separation of photogenerated electron-hole pairs in distinct monolayers, which is results in water splitting and will produces H_2 and O_2 gases under solar spectrum radiations. Furthermore, our objective is to improve the quality of our theoretical results by taking nonlinearity effects [61] into account and subsequently validating these findings through experiments. In the final phase, we will proceed to manufacture the intended electronic devices, with the potential to bring about significant positive advancements in the electronics industry.

IV. CONCLUSION

To summarize, this study comprehensively investigated the structural, electronic, and optical properties of GaS and Zr_2CO_2-monolayers, as well as the Zr_2CO_2/GaS van der Waals heterostructure, employing both Generalized Gradient Approximation (GGA) and Heyd-Scuseria-Ernzerhof (HSE) exchange-correlation functionals. The negative formation energies, minimal lattice mismatch, and weak van der Waals interactions collectively indicate the feasibility of synthesizing the Zr_2CO_2/GaS van der Waals (vdW) heterostructure in diverse configurations through experimental methodologies.

The calculated GGA (HSE) bandgap values of GaS, Zr_2CO_2, and Zr_2CO_2(MD4)/GaS ($\phi = 0°$) are 2.54 eV (3.32 eV), 1.06 eV (2.28 eV), and 0.98 eV (2.18 eV), respectively. The quasi-particle bandgap values for Zr_2CO_2 and GaS-monolayers, 2.13 eV and 3.82 eV respectively, align closely with experimental values [47, 60]. Significantly, the construction of the Zr_2CO_2/GaS vdW heterostructure improves the bandgap of the Zr_2CO_2-monolayer, leading to enhanced electronic and optical properties.

Our investigation also encompassed the analysis of complex dielectric function $\epsilon(\omega)$, EEL spectrum, $n(\omega)$, $k(\omega)$, and absorption coefficient for isolated GaS and Zr_2CO_2-monolayers, as well as the Zr_2CO_2/GaS vdW heterostructure. The Zr_2CO_2-monolayers displayed a blue shift in the first peak of the reflectivity and absorption spectra upon heterostructure formation. This shift indicates type-II band alignment under 3% biaxial compressive strain, fulfilling the requirements for photocatalytic water splitting, where GaS (Zr_2CO_2)-monolayer serves as the electron acceptor (donor). This unique feature enhances the separation and conduction of photogenerated electron-hole pairs across different monolayers, a fundamental prerequisite for water splitting under solar spectrum irradiation. These findings are consistent with experimental and theoretical works in the field, such as h-BN/C2N van der Waals heterostructures [62], TMDs/Mg(OH)$_2$ van der Waals heterostructures [63] and TMDs/BP van der Waals heterostructures [64].

Moreover, the built-in electric field formed at the heterostructure interface contributes to enhanced photocatalytic efficiency. Our predictions also suggest that the Zr_2CO_2/GaS vdW heterostructure holds promise as a photocatalyst [62, 63] and is highly desirable for photoelectric devices within the visible spectrum [63]. These results offer valuable guidance for the synthesis of Zr_2CO_2-monolayers and their potential applications as photocatalysts. This work paves the way for practical applications of 2D semiconducting materials in various real-world applications, including photocatalytic devices, photodiodes, photosensors, and batteries.

More generally, starting the integration of 2D materials with substrates on monolayers renowned for their high sensitivity to external influences allows for the application of this method in quantifying the state overlap between them. This scheme leads to valuable insights into the underlying electronic state of the system. For instance, it becomes evident that 2D materials exhibit heightened sensitivity to perturbations near critical points. Consequently, assessing the degree of overlap between substrates and monolayers with slightly varied system parameters serves as a meticulous tool for probing critical phenomena [65–67]. Moreover, when scrutinizing the overlap between substrates and monolayers undergoing non-equilibrium transformations induced by different perturbations, this approach offers a valuable means of investigating temporal correlation functions within non-equilibrium dynamics.

Therefore, this research provides valuable guidance for future efforts in synthesizing Zr_2CO_2 monolayers and underscores their potential applications in photocatalysis, photodiodes, photosensors, and batteries. The outcomes of this work set the stage for practical utilization of 2D semiconducting materials in real-world applications, paving the way for innovative solutions in renewable energy and optoelectronics.

V. AUTHORSHIP CONTRIBUTION STATEMENT

All authors contributed equally. M. Abdul played a crucial role in conducting an extensive literature review and performing the theoretical calculations. AUR and JB (an experimental physicist) were responsible for the computational methodology, data plotting, manuscript writing and review. They also actively participated in the experimental realization and provided supervision. Jehan, Qammer, and Bao were involved in the supervision, conceptualization, and manuscript review and editing. They also contributed to the project's administration.

This collaborative effort reflects the combined expertise and contributions of all authors to the successful completion of this study.

VI. CONFLICT OF INTEREST

We have no conflict of interest for this work to be declared.

VII. DATA AVAILABILITY STATEMENT

The data that support the findings of this study are available from the corresponding author upon reasonable request.

VIII. ACKNOWLEDGMENTS

REFERENCES

[1] N. C. Frey, J. Wang, G. I. Vega Bellido, B. Anasori, Y. Gogotsi, V. B. Shenoy, Prediction of synthesis of 2d metal carbides and nitrides (mxenes) and their precursors with positive and unlabeled machine learning, ACS nano 13 (3) (2019) 3031–3041.

[2] B. Anasori, M. R. Lukatskaya, Y. Gogotsi, 2d metal carbides and nitrides (mxenes) for energy storage, Nature Reviews Materials 2 (2) (2017) 1–17.

[3] M. Khazaei, A. Mishra, N. S. Venkataramanan, A. K. Singh, S. Yunoki, Recent advances in mxenes: from fundamentals to applications, Current Opinion in Solid State and Materials Science 23 (3) (2019) 164–178.

[4] M. Naguib, V. N. Mochalin, M. W. Barsoum, Y. Gogotsi, 25th anniversary article: Mxenes: a new family of two-dimensional materials, Advanced materials 26 (7) (2014) 992–1005.

[5] G. Deysher, C. E. Shuck, K. Hantanasirisakul, N. C. Frey, A. C. Foucher, K. Maleski, A. Sarycheva, V. B. Shenoy, E. A. Stach, B. Anasori, et al., Synthesis of mo4valc4 max phase and two-dimensional mo4vc4 mxene with five atomic layers of transition metals, ACS nano 14 (1) (2019) 204–217.

[6] M. Naguib, M. Kurtoglu, V. Presser, J. Lu, J. Niu, M. Heon, L. Hultman, Y. Gogotsi, M. W. Barsoum, Two-dimensional nanocrystals produced by exfoliation of ti3alc2, Advanced materials 23 (37) (2011) 4248–4253.

[7] M. Khazaei, M. Arai, T. Sasaki, C.-Y. Chung, N. S. Venkataramanan, M. Estili, Y. Sakka, Y. Kawazoe, Novel electronic and magnetic properties of two-dimensional transition metal carbides and nitrides, Advanced Functional Materials 23 (17) (2013) 2185–2192.

[8] A. Champagne, J.-C. Charlier, Physical properties of 2d mxenes: from a theoretical perspective, Journal of Physics: Materials 3 (3) (2020) 032006.

[9] J. Wang, T.-N. Ye, Y. Gong, J. Wu, N. Miao, T. Tada, H. Hosono, Discovery of hexagonal ternary phase ti 2 inb 2 and its evolution to layered boride tib, Nature communications 10 (1) (2019) 1–8.

[10] N. Miao, J. Wang, Y. Gong, J. Wu, H. Niu, S. Wang, K. Li, A. R. Oganov, T. Tada, H. Hosono, Computational prediction of boron-based max phases and mxene derivatives, Chemistry of Materials 32 (16) (2020) 6947–6957.

[11] Y. Yue, B. Wang, N. Miao, C. Jiang, H. Lu, B. Zhang, Y. Wu, J. Ren, M. Wang, Tuning the magnetic properties of zr2n mxene by biaxial strain, Ceramics International 47 (2) (2021) 2367–2373.

[12] X.-H. Li, X.-H. Cui, C.-H. Xing, H.-L. Cui, R.-Z. Zhang, Strain-tunable electronic and optical properties of zr2co2 mxene and mose2 van der waals heterojunction: A first principles calculation, Applied Surface Science 548 (2021) 149249.

[13] M. R. Lukatskaya, B. Dunn, Y. Gogotsi, Multidimensional materials and device architectures for future hybrid energy storage, Nature communications 7 (1) (2016) 1–13.

[14] J. Pang, R. G. Mendes, A. Bachmatiuk, L. Zhao, H. Q. Ta, T. Gemming, H. Liu, Z. Liu, M. H. Rummeli, Applications of 2d mxenes in energy conversion and storage systems, Chemical Society Reviews 48 (1) (2019) 72–133.

[15] H. Wang, Y. Wu, X. Yuan, G. Zeng, J. Zhou, X. Wang, J. W. Chew, Clay-inspired mxene-based electrochemical devices and photo-electrocatalyst: state-of-the-art progresses and challenges, Advanced Materials 30 (12) (2018) 1704561.

[16] J. Zhu, E. Ha, G. Zhao, Y. Zhou, D. Huang, G. Yue, L. Hu, N. Sun, Y. Wang, L. Y. S. Lee, et al., Recent advance in mxenes: a promising 2d material for catalysis, sensor and chemical adsorption, Coordination Chemistry Reviews 352 (2017) 306–327.

[17] K. Hantanasirisakul, Y. Gogotsi, Electronic and optical properties of 2d transition metal carbides and nitrides (mxenes), Advanced materials 30 (52) (2018) 1804779.

[18] F. Ghafoor, M. Arfan, A. U. Rahman, M. A. Rafiq, et al., Enhanced electronic and thermoelectric properties of zr2co2/gas van der waals heterostructure: A first-principles study, Surfaces and Interfaces 35 (2022) 102453.

[19] S. Kumar, U. Schwingenschlögl, Thermoelectric performance of functionalized sc 2 c mxenes, Physical review B 94 (3) (2016) 035405.

[20] A. K. Geim, I. V. Grigorieva, Van der waals heterostructures, Nature 499 (7459) (2013) 419–425.

[21] H. Ullah, A. U. Rahman, E. L. Aragão, F. F. A. Barbosa, K. G. R. Pergher, R. Giulian, H. C. Júnior, R. L. Sommer, S. Khan, Homogeneous v incorporation via single-step anodization: Structural doping or heterostructure formation?, Applied Surface Science 556 (2021) 149694.

[22] A. U. Rahman, J. M. Morbec, G. Rahman, P. Kratzer, Commensurate versus incommensurate heterostructures of group-iii monochalcogenides, Physical Review Materials 2 (9) (2018) 094002.

[23] B. G. Levi, Simple compound manifests record-high thermoelectric performance, Physics today 67 (6) (2014) 14.

[24] A. D. LaLonde, Y. Pei, H. Wang, G. J. Snyder, Lead telluride alloy thermoelectrics, Materials today 14 (11) (2011) 526–532.

[25] A. M. Dehkordi, M. Zebarjadi, J. He, T. M. Tritt, Thermoelectric power factor: Enhancement mechanisms and strategies for higher performance thermoelectric materials, Materials Science and Engineering: R: Reports 97 (2015) 1–22.

[26] W. Kohn, L. J. Sham, Self-consistent equations including exchange and correlation effects, Physical review 140 (4A) (1965) A1133.

[27] P. Giannozzi, S. Baroni, N. Bonini, M. Calandra, R. Car, C. Cavazzoni, D. Ceresoli, G. L. Chiarotti, M. Cococcioni, I. Dabo, et al., QUANTUM ESPRESSO: a modular and open-source software project for quantum simulations of materials, Journal of physics: Condensed matter 21 (39) (2009) 395502.

[28] J. P. Perdew, K. Burke, M. Ernzerhof, Generalized gradient approximation made simple, Physical review letters 77 (18) (1996) 3865.

[29] H. J. Monkhorst, J. D. Pack, Special points for Brillouin-zone integrations, Physical review B 13 (12) (1976) 5188.

[30] J. Heyd, G. E. Scuseria, M. Ernzerhof, Hybrid functionals based on a screened coulomb potential, The Journal of chemical physics 118 (18) (2003) 8207–8215.

[31] T. Kaewmaraya, M. Ramzan, H. Löfås, R. Ahuja, Hybrid density functional study of electronic and optical properties of phase change memory material: Ge 2 sb 2 te 5, Journal of Applied Physics 113 (3) (2013) 033510.

[32] M. Khan, A. Kashyap, A. Solanki, T. Nautiyal, S. Auluck, Interband optical properties of Ni_3Al, Physical Review B 48 (23) (1993) 16974.

[33] F. Wooten, Optical properties of solids, American Journal of Physics 41 (7) (1973) 939–940.

[34] N. V. Smith, Photoelectron energy spectra and the band structures of the noble metals, Physical Review B 3 (6) (1971) 1862.

[35] C. Ambrosch-Draxl, J. O. Sofo, Linear optical properties of solids within the full-potential linearized augmented planewave method, Computer physics communications 175 (1) (2006) 1–14.

[36] M. Fox, Optical properties of solids: Oxford university press (2001).

[37] F. Kong, G. Jiang, Nonlinear optical response of wurtzite ZnO from first principles, Physica B: Condensed Matter 404 (16) (2009) 2340–2344.

[38] S. Singh, Refractive index measurement and its applications, Physica Scripta 65 (2) (2002) 167.

[39] S. Kasap, Springer handbook of electronic and photonic materials, Springer Science & Business Media, 2006.

[40] P. Rani, G. S. Dubey, V. Jindal, DFT study of optical properties of pure and doped graphene, Physica E: Low-dimensional Systems and Nanostructures 62 (2014) 28–35.

[41] S. Grimme, Semiempirical gga-type density functional constructed with a long-range dispersion correction, Journal of computational chemistry 27 (15) (2006) 1787–1799.

[42] F. S. Galasso, F. C. Douglas, R. J. Kasper, Relationship between magnetic curie points and cell sizes of solid solutions with the ordered perovskite structure, The Journal of Chemical Physics 44 (4) (1966) 1672–1674.

[43] S. Khan, B. Amin, L.-Y. Gan, I. Ahmad, Strain engineering of electronic structures and photocatalytic responses of mxenes functionalized by oxygen, Physical Chemistry Chemical Physics 19 (22) (2017) 14738–14744.

[44] C. Hu, X. Yu, Y. Li, J. Cheng, Q. Li, B. Xiao, Bandgap engineering of strained s-terminated mxene and its promising application as nox gas sensor, Applied Surface Science 592 (2022) 153296.

[45] R. Khan, A. U. Rahman, Q. Zhang, P. Kratzer, S. M. Ramay, First-principles computational exploration of ferromagnetism in monolayer GaS via substitutional doping, Journal of Physics: Condensed Matter 33 (2021) 314003.

[46] Y. He, M. Zhang, J.-j. Shi, Y.-l. Cen, M. Wu, Improvement of visible-light photocatalytic efficiency in a novel inse/zr2co2 heterostructure for overall water splitting, The Journal of Physical Chemistry C 123 (20) (2019) 12781–12790.

[47] Y. Zhang, W. Xia, Y. Wu, P. Zhang, Prediction of mxene based 2d tunable band gap semiconductors: Gw quasiparticle calculations, Nanoscale 11 (9) (2019) 3993–4000.

[48] S. Demirci, N. Avazlı, E. Durgun, S. Cahangirov, Structural and electronic properties of monolayer group iii monochalcogenides, Physical Review B 95 (11) (2017) 115409.

[49] C. Chen, X. Xie, B. Anasori, A. Sarycheva, T. Makaryan, M. Zhao, P. Urbankowski, L. Miao, J. Jiang, Y. Gogotsi, Mos2-on-mxene heterostructures as highly reversible anode materials for lithium-ion batteries, Angewandte Chemie International Edition 57 (7) (2018) 1846–1850.

[50] Z. Guan, C.-S. Lian, S. Hu, S. Ni, J. Li, W. Duan, Tunable structural, electronic, and optical properties of layered two-dimensional c2n and mos2 van der waals heterostructure as photovoltaic material, The Journal of Physical Chemistry C 121 (6) (2017) 3654–3660.

[51] T. Cheiwchanchamnangij, W. R. Lambrecht, Quasiparticle band structure calculation of monolayer, bilayer, and bulk mos 2, Physical Review B 85 (20) (2012) 205302.

[52] Z. Zhang, M. Si, S. Peng, F. Zhang, Y. Wang, D. Xue, Bandgap engineering in van der waals heterostructures of blue phosphorene and mos2: A first principles calculation, Journal of Solid State Chemistry 231 (2015) 64–69.

[53] A. U. Rahman, G. Rahman, P. Kratzer, Enhanced electronic and magnetic properties by functionalization of monolayer gas via substitutional doping and adsorption, Journal of Physics: Condensed Matter 30 (19) (2018) 195805.

[54] A. U. Rahman, H. Ullah, A. Jamil, Z. Iqbal, M. Naveed-Ul-Haq, Robust ferromagnetism and half-metallicity in hydrogenated monolayer-cds, Physica B: Condensed Matter 570 (2019) 209–216.

[55] P. Yadav, P. D. Bhuyan, S. Rout, Y. Sonvane, S. K. Gupta, E. Sinha, Correlation between experimental and theoretical study of scheelite and wolframite-type tungstates, Materials Today Communications 25 (2020) 101417.

[56] M. Bernardi, M. Palummo, J. C. Grossman, Extraordinary sunlight absorption and one nanometer thick photovoltaics using two-dimensional monolayer materials, Nano letters 13 (8) (2013) 3664–3670.

[57] H. Sun, Z. Wang, Y. Wang, Band alignment of two-dimensional metal monochalcogenides mxs (m= ga, in; x= s, se, te), AIP Advances 7 (9) (2017).

[58] Y. Fan, X. Ma, X. Liu, J. Wang, H. Ai, M. Zhao, Theoretical design of an inse/gate vdw heterobilayer: A potential visible-light photocatalyst for water splitting, The Journal of Physical Chemistry C 122 (49) (2018) 27803–27810.

[59] Y. Qu, X. Duan, Progress, challenge and perspective of heterogeneous photocatalysts, Chemical Society Reviews 42 (7) (2013) 2568–2580.

[60] H. L. Zhuang, R. G. Hennig, Single-layer group-iii monochalcogenide photocatalysts for water splitting, Chemistry of Materials 25 (15) (2013) 3232–3238.

[61] M. Abdul, A. U. Rahman, B. Jing, Effects of thermal fluctuation when an optical cavity possesses neutral atoms and a two-mode laser system, Chaos, Solitons & Fractals 168 (2023) 113162.

[62] G. Wang, Z. Li, W. Wu, H. Guo, C. Chen, H. Yuan, S. A. Yang, A two-dimensional h-bn/c 2 n heterostructure as a promising metal-free photocatalyst for overall water-splitting, Physical Chemistry Chemical Physics 22 (42) (2020) 24446–24454.

[63] Y. Luo, S. Wang, K. Ren, J.-P. Chou, J. Yu, Z. Sun, M. Sun, Transition-metal dichalcogenides/mg (oh) 2 van der waals heterostructures as promising water-splitting photocatalysts: a first-principles study, Physical Chemistry Chemical Physics 21 (4) (2019) 1791–1796.

[64] K. Ren, M. Sun, Y. Luo, S. Wang, J. Yu, W. Tang, First-principle study of electronic and optical properties of two-dimensional materials-based heterostructures based on transition metal dichalcogenides and boron phosphide, Applied Surface Science 476 (2019) 70–75.

[65] P. Zanardi, N. Paunković, Ground state overlap and quantum phase transitions, Phys. Rev. E 74 (2006) 031123.

[66] J. H. S. Antonio Gaetano Ricciardulli, Sheng Yang, M. Saliba, Emerging perovskite monolayers, Nature Materials 20 (2021) 1325–1336.

[67] E. P. C. J. M. A. D. F. T. G. T. K. Y. I. A. V. P. J. A. Z. C. W. Z. I. A. L.-J. L. U. E. A. N. B. T. D. A. Saptarshi Das, Amritanand Sebastian, R. Singh, Transistors based on two-dimensional materials for future integrated circuits, Nature Electronics 04 (2021) pages786–799.

Supplementary Files

This is a list of supplementary files associated with this preprint. Click to download.

- SI.pdf